ARTICLES
https://doi.org/10.1038/s41590-018-0094-2

nature immunology

Corrected: Author Correction

γδ T cells producing interleukin-17A regulate adipose regulatory T cell homeostasis and thermogenesis

Ayano C. Kohlgruber[1,2], Shani T. Gal-Oz[3], Nelson M. LaMarche[1,2], Moto Shimazaki[1], Danielle Duquette[4], Hui-Fern Koay[5,6], Hung N. Nguyen[1], Amir I. Mina[4], Tyler Paras[1], Ali Tavakkoli[7], Ulrich von Andrian[2,8], Adam P. Uldrich[5,6], Dale I. Godfrey[5,6], Alexander S. Banks[4], Tal Shay[3], Michael B. Brenner[1,10*] and Lydia Lynch[1,4,9,10*]

γδ T cells are situated at barrier sites and guard the body from infection and damage. However, little is known about their roles outside of host defense in nonbarrier tissues. Here, we characterize a highly enriched tissue-resident population of γδ T cells in adipose tissue that regulate age-dependent regulatory T cell (T_{reg}) expansion and control core body temperature in response to environmental fluctuations. Mechanistically, innate PLZF$^+$ γδ T cells produced tumor necrosis factor and interleukin (IL) 17 A and determined PDGFRα$^+$ and Pdpn$^+$ stromal-cell production of IL-33 in adipose tissue. Mice lacking γδ T cells or IL-17A exhibited decreases in both ST2$^+$ T_{reg} cells and IL-33 abundance in visceral adipose tissue. Remarkably, these mice also lacked the ability to regulate core body temperature at thermoneutrality and after cold challenge. Together, these findings uncover important physiological roles for resident γδ T cells in adipose tissue immune homeostasis and body-temperature control.

Adipose tissue contains a unique immunological compartment that is important for physiologic responses to fasting and feeding, regulation of body weight, and thermogenesis. In adipose tissue, compared with lymphoid organs, approximately 80–90% of the immune system is innate. Much of what is known about the adipose tissue immune system suggests that its major roles are not focused on fighting infection. Instead, obesity studies have revealed that perturbations in immune cells or signaling molecules can either protect against or contribute to inflammation and insulin sensitivity. Although it is less understood, the resident innate immune compartment of adipose tissue also probably has important functions in the absence of obesity.

Beyond innate myeloid cells, a substantial component of adipose tissue comprises innate lymphocytes such as type 2 innate lymphoid cells (ILC2s), invariant natural killer T (*i*NKT) cells, mucosal-associated invariant T cells, natural killer (NK) cells, and γδ T cells[1,2]. In the lean state, ILC2s and *i*NKT cells are critical for maintaining an anti-inflammatory environment through secretion of type 2 cytokines that support the function and survival of eosinophils, alternatively activated macrophages, and T_{reg} cells[3–6]. Moreover, under other conditions including cold challenge, ILC2s and *i*NKT cells can induce thermogenic programs in adipose tissue[7,8]. In contrast, in obesity, NK[8,9] cells and mucosal-associated invariant T cells[10–12] secrete proinflammatory cytokines that impair glucose handling by adipocytes, hepatocytes, and muscle cells, and interfere with insulin production and insulin signaling. Despite recent advances in the understanding of adipose innate lymphocytes, the roles of γδ T cells in this dynamic organ remain largely unknown.

Foxp3$^+$ T_{reg} cells are a key adaptive cell type in adipose tissue. T_{reg} cells are low in number in adipose tissue in mice until 20 weeks of age, after which they greatly expand and compose 40–80% of the CD4$^+$ T cell population[9–12]. Adipose T_{reg} cells have enhanced expression of genes, such as *Il10*, *Gata3*, *Pparg*, and *Ilrl1*, that define their adipose and anti-inflammatory phenotype[9,10,13,14]. Furthermore, they express high amounts of the IL-33 receptor ST2 (also known as IL-1R4), and IL-33 is critical for their local expansion and transcriptional stability[11,15]. We previously described a critical role of *i*NKT-cell-derived IL-2 in maintaining T_{reg} cell numbers and boosting their function in adipose tissue[3]. In addition, ILC2s have been shown to play a role in T_{reg} cell homeostasis via inducible T cell co-stimulator–ligand interactions after IL-33 administration, and T_{reg} cells from mice deficient in inducible T cell co-stimulator ligand do not expand after IL-33 treatment[16]. Although these studies have provided mechanistic insights into the regulation of T_{reg} homeostasis, the basis for the marked increase in T_{reg} cell numbers with age is unknown.

IL-33 is an important factor in nonshivering thermogenesis, a metabolic adaptation to cold temperatures[17,18]. Adaptive thermogenesis is mediated largely by uncoupling protein 1 (UCP1), which uncouples oxidative phosphorylation from ATP synthesis, thereby generating heat. IL-33 is critical for body-temperature regulation in newborns[18], and adult mice deficient in IL-33 cannot induce UCP1

[1]Division of Rheumatology, Immunology and Allergy, Brigham and Women's Hospital, Boston, MA, USA. [2]Division of Medical Sciences, Harvard Medical School, Boston, MA, USA. [3]Department of Life Sciences, Ben-Gurion University of the Negev, Beersheba, Israel. [4]Division of Endocrinology, Department of Medicine, Brigham and Women's Hospital, Boston, MA, USA. [5]Department of Microbiology and Immunology, Peter Doherty Institute for Infection and Immunity, University of Melbourne, Parkville, Australia. [6]ARC Centre of Excellence in Advanced Molecular Imaging, University of Melbourne, Parkville, Australia. [7]Department of General and Gastrointestinal Surgery, Brigham and Women's Hospital, Boston, MA, USA. [8]Department of Microbiology and Immunology, Harvard Medical School, Boston, MA, USA. [9]School of Biochemistry and Immunology, Trinity College, Dublin, Ireland. [10]These authors jointly supervised this work: Michael B. Brenner and Lydia Lynch. *e-mail: mbrenner@research.bwh.harvard.edu; llynch@bwh.harvard.edu

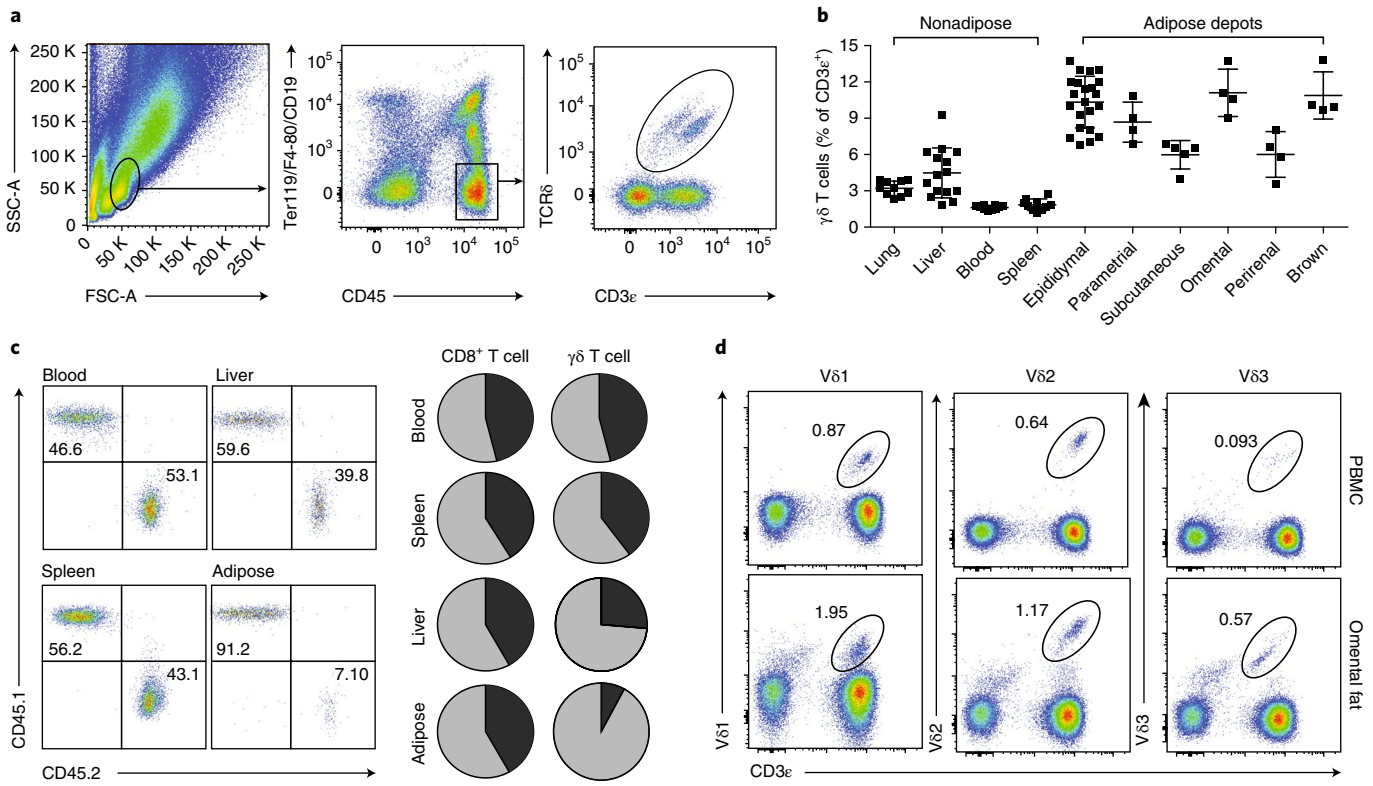

Fig. 1 | γδ T cells are enriched and resident in adipose tissue. a, Representative flow cytometry plots of γδ T cells from the epididymal WAT stromal vascular fraction (eWAT SVF). K denotes thousand. **b**, Frequency of γδ T cells across various adipose tissue depots as a percentage of CD3ε$^+$ T cells in male eWAT ($n \geq 4$ mice per group). Each symbol represents an individual mouse; small horizontal lines indicate the mean. **c**, Flow cytometry of lymphocytes in the blood, liver, spleen, and adipose tissue of CD45.1$^+$ and CD45.2$^+$ congenic C57BL/6 parabiotic pairs joined at 6 weeks of age and analyzed 2 weeks later (left); and frequency pie charts of CD45.1$^+$ and CD45.2$^+$ CD8$^+$ and γδ T cells (right). **d**, Frequency of Vδ1$^+$, Vδ2$^+$, and Vδ3$^+$ γδ T cells (% of CD45$^+$PI$^-$ cells) in peripheral blood (PBMCs) or from matched omental fat from patients before bariatric surgery. Data are representative of three experiments (**a**,**b**,**d**; mean ± s.e.m. in **b**) or one experiment (**c**).

and consequently exhibit defects in thermogenesis[8,19]. In adipose tissue, the main source of IL-33 is debated and has been ascribed to a number of different stromal cell types including mesenchymal Cadherin-11$^+$ (Cdh11) cells, podoplanin$^+$ (Pdpn$^+$) fibroblasts, or CD31$^+$ endothelial cells[15,16,20,21]. Importantly, the mechanisms that regulate the endogenous expression of IL-33 in adipose tissue remain elusive.

Here, we describe an unexpected role of a canonical IL-17A-producing adipose-resident γδ T cell population that is required for age-dependent increases in T_{reg} cells and the maintenance of body temperature and thermogenic tenor.

Results

γδ T cells are enriched and resident in adipose tissue. We profiled visceral adipose tissue through flow cytometry and found that γδ T cells were highly enriched in adipose tissue compared with other organs (Fig. 1a,b). γδ T cells were more abundant across several adipose depots than in peripheral sites including the lung, liver, blood, and spleen (Fig. 1b). To determine whether the enriched population of γδ T cells in visceral adipose tissue was constantly replenished from the periphery or whether these cells represented a tissue-resident population, we performed parabiosis experiments on congenic CD45.1 and CD45.2 mice (Fig. 1c). Whereas CD8$^+$ T cells reached near-complete chimerism for the blood, spleen, liver, and adipose tissue, γδ T cells showed full recirculation only in the blood and spleen, whereas the liver and, more strikingly, the adipose tissue showed less chimerism (Fig. 1c). In adipose tissue, >90% of γδ T cells were endogenous to the host mice, thus indicating a resident or long-dwelling phenotype. Importantly, γδ T cells, identified by their Vδ chain usage, were also found in human omental adipose tissue (Fig. 1d). In human omentum, compared with peripheral blood, Vδ1, Vδ2, and Vδ3 subsets accounted for higher percentages of CD45$^+$ lymphocytes. Thus, γδ T cells are enriched and resident in mouse and human adipose tissues.

PLZF discriminates two γδ T cell populations. When profiling γδ T cells in adipose tissue, we found that they could be separated into two distinct populations on the basis of CD3ε intensity[22] (Fig. 2a). CD3ε^{hi} γδ T cells were more abundant than CD3ε^{lo} cells in adipose tissue, making up to two-thirds of the total γδ T cell pool, whereas other organs such as the liver and spleen had few CD3ε^{hi} cells (Fig. 2a). CD27, a member of the TNFR superfamily and a costimulatory molecule, demarcates functionally distinct γδ subsets in mice[23]. We found that adipose γδ T cells were largely CD27$^-$, corresponding to the CD3ε^{hi} subset, whereas in the spleen and liver, γδ T cells were largely CD3ε^{lo}CD27$^+$ (Fig. 2b). Additional phenotyping indicated that the enriched population of CD3ε^{hi}CD27$^-$ γδ T cells was CD69^{hi} CD44^{hi}CD127$^+$CD45RB$^-$ (Fig. 2c).

The BTB-POZ transcription factor PLZF, encoded by *Zbtb16*, imparts innate-like qualities to lymphocytes. PLZF is expressed on certain γδ T cells from other organs[24,25], *i*NKT cells[26], and human mucosal-associated invariant T cells[27]. We analyzed PLZF expression in adipose γδ T cells through flow cytometry and found that CD3ε^{hi} γδ T cells, compared with CD3ε^{lo} cells, highly expressed PLZF (Fig. 2d). PLZF expression was significantly higher in CD3ε^{hi} γδ T cells in the adipose tissue than in the liver and spleen (Fig. 2d). Furthermore, using *Zbtb16*^{GFP} mice, we found that almost all the PLZF signal (>92% of PLZF$^+$ cells) from adipose CD45$^+$ cells

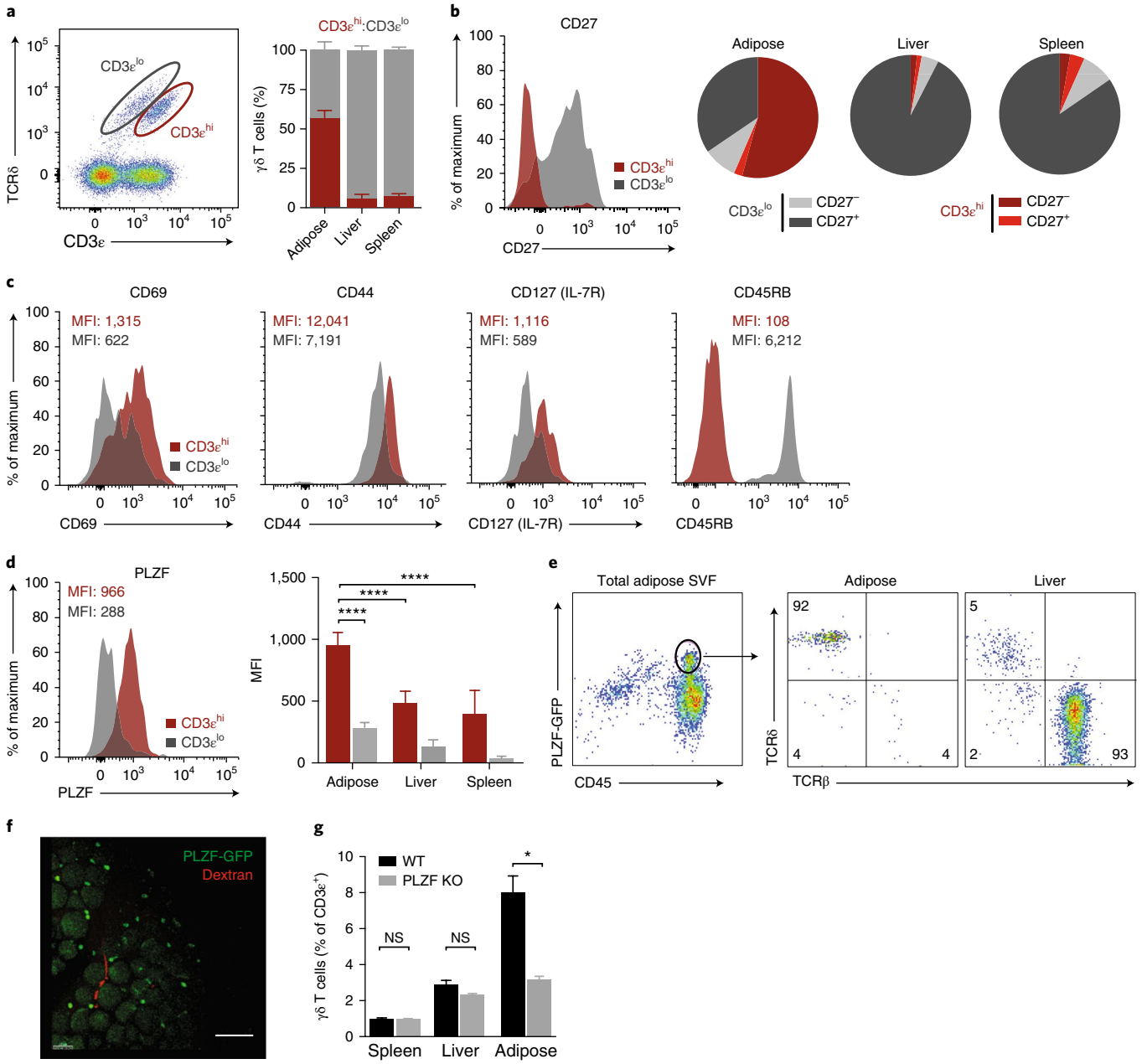

Fig. 2 | PLZF discriminates two γδ T cell populations. a, Representative flow cytometry and frequency quantification of CD3ε^{hi} and CD3ε^{lo} γδ T cells from eWAT SVF across adipose, liver, and spleen ($n = 5$ mice). **b**, CD27 expression by CD3ε^{hi} and CD3ε^{lo} γδ T cells (left) and subset quantification from adipose, liver, and spleen (right) ($n = 5$ mice). **c**, Representative histograms of mean fluorescence intensity (MFI) of CD69, CD44, CD127, and CD45RB expression by CD3ε^{hi} and CD3ε^{lo} γδ T cells. **d**, Representative histogram of PLZF expression by CD3ε^{hi} and CD3ε^{lo} γδ T cells (left) and MFI quantification across adipose, liver, and spleen (right) ($n = 5$ mice). **e**, Representative flow cytometry and quantification of TCRβ^{+} versus TCRδ^{+} cells of PLZF^{+}CD45^{+} cells from eWAT SVF. **f**, Immunofluorescence microscopy of whole-mount adipose tissue from *Zbtb16*^{GFP} mice (green) injected with dextran (red). Scale bar, 100 µm. **g**, Frequency of γδ T cells from wild-type (WT) and *Zbtb16*$^{-/-}$ mice ($n = 5$). KO, knockout. NS, not significant ($P > 0.05$); $^{*}P < 0.05$; $^{****}P < 0.0001$ (one-way ANOVA). Data are representative of three experiments (**a**–**e**; mean ± s.e.m. in **a**,**d**) or two experiments (**f**,**g**; mean ± s.e.m. in **g**).

was attributable to γδ T cells, whereas in the liver, most of the PLZF^{+}CD45^{+} lymphocytes were TCRβ^{+} cells (Fig. 2e). Whole-mount staining of adipose tissue from *Zbtb16*^{GFP} mice further confirmed the presence of PLZF^{+} cells and revealed them to be interspersed among adipocytes (Fig. 2f). PLZF-deficient (Luxoid) mice showed a two-thirds decrease in the frequency of adipose γδ T cells, corresponding to the relative frequency of PLZF^{+}CD3ε^{hi} γδ T cells in adipose tissue (Fig. 2g). γδ T cell frequencies in other organs were unaffected by the loss of PLZF, because fewer PLZF^{+}CD3ε^{hi} γδ T cells were present (Fig. 2g), thus highlighting the requirement of PLZF for the CD27^{-} γδ T cell population resident in adipose tissue.

γδ T cells are important for adipose T_{reg} accumulation. Next, we quantified the numbers of γδ T cells to determine changes in their frequency in adipose tissue over time. Interestingly, γδ T cells displayed accumulation kinetics similar to those of Foxp3^{+} T_{reg} cells in adipose tissue (Fig. 3a). In contrast, both ILC2s and *i*NKT cells, two populations previously shown to influence adipose T_{reg} numbers, decreased at the time of T_{reg} expansion (Fig. 3b). Beyond

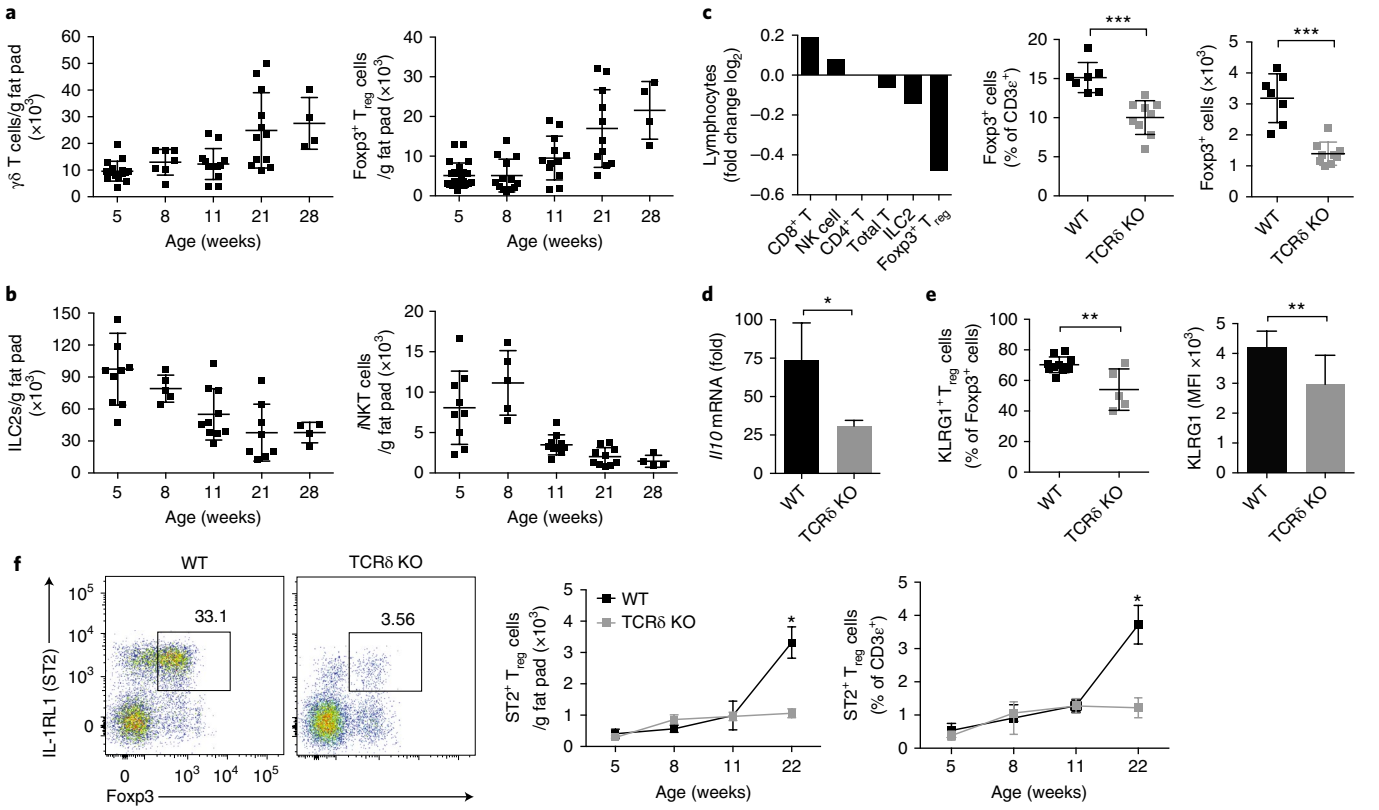

Fig. 3 | γδ T cells are important for adipose T_{reg} accumulation. a,**b**, Numbers per gram eWAT of γδ T and Foxp3$^+$ T_{reg} cells (**a**) and ILC2s and *i*NKT cells (**b**) at 5, 8, 11, 21, and 28 weeks of age ($n \geq 4$ mice per time point). **c**, Ratio ($\log_2$ normalized fold change) of CD8$^+$ T, NK, CD4$^+$ T, ILC2s, and T_{reg} cell numbers from *Tcrd*$^{-/-}$ mice compared with WT mice (left) at 16 weeks of age ($n = 10$ mice). Frequency and numbers of Foxp3$^+$ T_{reg} cells in eWAT between WT and *Tcrd*$^{-/-}$ mice (right) at 16 weeks ($n = 4$ mice per group). **d**, Quantitative real-time PCR for *Il10* expression normalized to *Tbp* from sorted CD25$^+$CD4$^+$ T_{reg} cells from WT and *Tcrd*$^{-/-}$ mice at 16 weeks ($n = 5$ mice). **e**, Frequency (left) and MFI (right) of cell-surface KLRG1 expression on eWAT Foxp3$^+$ T_{reg} cells from mice 16 weeks of age ($n = 5$ mice). **f**, Representative flow cytometry of ST2$^+$Foxp3$^+$ T_{reg} cells from eWAT (left) and cell numbers from WT and *Tcrd*$^{-/-}$ littermate (right) mice ($n = 5$) at 5, 8, 11, and 22 weeks of age. Each symbol represents an individual mouse; small horizontal lines indicate the mean. NS, not significant ($P > 0.05$); $^*P < 0.05$; $^{**}P < 0.01$; $^{***}P < 0.001$. (Two-tailed Student's *t* test in **c**–**e**; one-way ANOVA in **f**). Data are representative of three experiments (**a**,**b**,**f**; mean ± s.e.m. in **a**,**b**,**f**) or two experiments (**c**–**e**; mean ± s.e.m. in **c**–**e**).

T_{reg} cells and γδ T cells, no other quantified lymphocyte population increased with age (Supplementary Fig. 1). T_{reg} cells are well known to expand in adipose tissue with age, but a unifying mechanism explaining their temporal accumulation remains unknown. Thus, we wondered whether γδ T cells might play a role in adipose T_{reg} homeostasis. To test this possibility, we profiled wild-type mice and mice deficient in T cell receptor (TCR) delta (*Tcrd*$^{-/-}$). We found that the frequency of T_{reg} cells was significantly lower in *Tcrd*$^{-/-}$ mice than in their wild-type counterparts at 20 weeks of age (Fig. 3c). A characteristic feature of adipose T_{reg} cells is their high expression of IL-10 and the receptor proteins KLRG1 and ST2 (ref. [10]). T_{reg} cells sorted from *Tcrd*$^{-/-}$ adipose tissue expressed significantly less *Il10* (Fig. 3d) and surface KLRG1 than did those sorted from wild-type adipose tissue (Fig. 3e). Finally, we found a striking defect in ST2$^+$ T_{reg} cell accumulation in *Tcrd*$^{-/-}$ mice compared with their wild-type littermates at 22 weeks of age, at the time of physiologic T_{reg} cell expansion (Fig. 3f). Together these results reveal a concomitant increase in γδ T cells and T_{reg} cells with age and a requirement of γδ T cells for visceral adipose T_{reg} accumulation.

PLZF$^+$ γδ T cells are innate IL-17A-producing cells. γδ T cells are generally recognized as innate-like lymphocytes that induce inflammation in response to pathogens and cellular stress. They rapidly secrete inflammatory cytokines such as TNF, IFN-γ, and IL-17, as well as chemokines that recruit key phagocytes to injured or infected tissues[28]. To understand how γδ T cells modulate T_{reg} numbers in adipose tissue, we sought to further characterize their transcriptional phenotype and function. PLZF$^+$ and PLZF$^-$ γδ T cells were sorted from adipose tissue from *Zbtb16*^{GFP} mice and subjected to RNA sequencing and gene-expression analysis. Differential expression analysis revealed 247 and 205 genes that were significantly upregulated in adipose PLZF$^+$ and PLZF$^-$ γδ T cells, respectively, of which the top 60 genes are shown (Fig. 4a). In accordance with the sorting strategy, *Zbtb16* was among the most differentially expressed genes (Fig. 4a,b). Notably, transcripts of genes including *Sox13*, *Rorc*, *Il1r1*, and *Il23r* were significantly higher in PLZF$^+$ γδ T cells than their PLZF$^-$ counterparts (Fig. 4a,b). Moreover, the high transcript levels of *Tcrg*, *Tcrd*, *Cd3e*, and *Cd3g* in PLZF$^+$ γδ T cells reaffirmed the flow cytometry data distinguishing the CD3ε^{hi} versus CD3ε^{lo} γδ subsets (Fig. 4a). In contrast, the PLZF$^-$ γδ T cells showed significantly higher expression of genes characteristic of NK cells, including *Ncr1*, *Nkg7*, *Klrk1*, *Gzmb*, and *Gzma* (Fig. 4a,b). The high expression of these genes, together with the overexpression of genes encoding the transcription factor T-bet (*Tbx21*) as well as CD27 (*Cd27*), highlight their type 1 helper T cell– and NK-like transcriptional phenotype (Fig. 4b). Finally, we validated the protein expression of the receptor RORγt and of T-bet in γδ T cells and found them to be discretely expressed by PLZF$^+$ and PLZF$^-$ subsets, respectively (Fig. 4c).

Transcriptional analysis revealed that PLZF$^+$ γδ T cells expressed *Il17a*, whereas PLZF$^-$ γδ T cells expressed *Ifng*. Because CD27 is useful to demarcate IL-17A-producing (CD27$^-$) versus

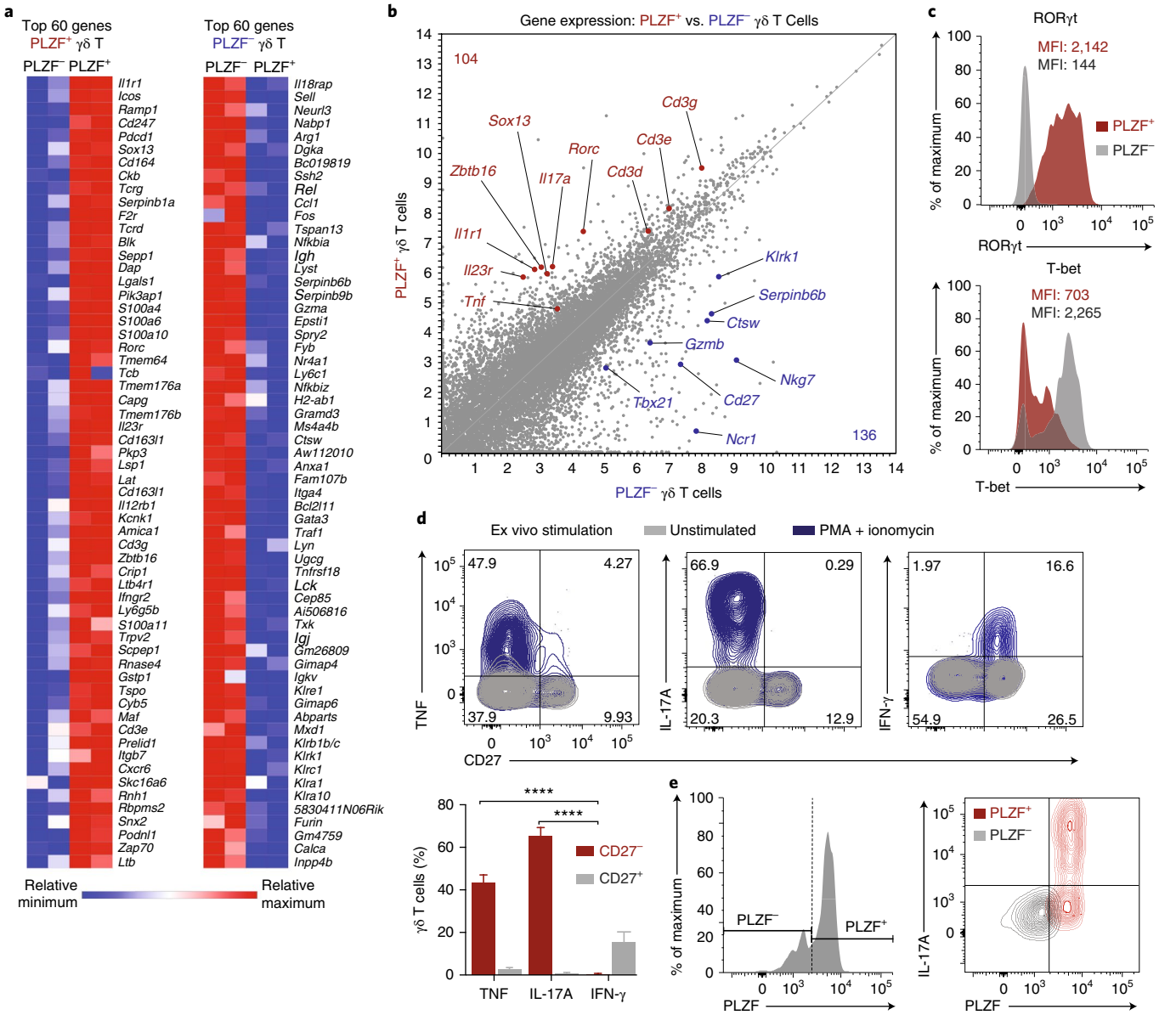

Fig. 4 | PLZF⁺ γδ T cells are innate-IL17A-producing cells. a, Heat map of the top 60 genes differentially expressed (false-discovery-rate-adjusted *P* value < 0.01) between PLZF⁺ (left) and PLZF⁻ (right) γδ T cells. **b**, Scatter plot of gene transcripts differentially expressed by PLZF⁺ and PLZF⁻ γδ T cells from 14-week-old male mice. **c**, Flow cytometry of RORγt (top) and T-bet (bottom) expression in PLZF⁺ and PLZF⁻ γδ T cells from eWAT SVF. **d**, Representative intracellular cytokine staining (top) and quantification (bottom) on gated γδ T cells from eWAT SVF for TNF, IL-17A, and IFN-γ after 4-h stimulation with PMA and ionomycin ($n = 4$ mice). **e**, Representative intracellular IL-17A staining of gated PLZF⁺ and PLZF⁻ γδ T cells from eWAT SVF after 4-h treatment with PMA and ionomycin ($n = 5$ mice). Small horizontal lines indicate the mean. NS, not significant ($P > 0.05$); *$P < 0.05$; **$P < 0.01$; ****$P < 0.0001$ (one-way ANOVA in **d**). Data are representative of two experiments (**c**–**e**; mean ± s.e.m. in **d**).

IFN-γ-producing (CD27⁺) γδ T cells, we used CD27 as a marker for functional analysis. After stimulation, PLZF⁺ γδ T cells produced exclusively IL-17A and TNF, whereas PLZF⁻ γδ T cells produced exclusively IFN-γ, results consistent with their gene expression (Fig. 4d,e). Together, our transcriptional, phenotypic, and functional characterizations highlight PLZF⁺ γδ T cells as innate IL-17A-producing cells and reveal an effector program distinct from that of the NK-like PLZF⁻ γδ T cells in adipose tissue.

ST2⁺ T_{reg} numbers depend on PLZF⁺ γδ T cells and IL-17A. To parse the relative contributions of the two γδ T cell populations to the observed T_{reg} phenotype, we determined the kinetics of accumulation of the two subsets over time (Fig. 5a). Flow cytometry analysis of visceral fat pads showed that IL-17A-producing PLZF⁺ γδ T cells, but not PLZF⁻ γδ T cells, expanded with age (Fig. 5a). Importantly, profiling γδ T cells from *Il17a*^{GFP} mice showed that the cell numbers significantly increased in adipose tissue with age (Fig. 5b). We next asked whether IL-17A might be important for the observed T_{reg} cell accumulation. We found that IL-17A-deficient (*Il17a*$^{-/-}$) mice, compared with wild-type mice, had significantly lower numbers and frequencies of total Foxp3⁺ T_{reg} cells and did not accumulate ST2⁺ T_{reg} cells in adipose tissue at 20 weeks of age (Fig. 5c). The *i*NKT and ILC2 numbers were not different between wild-type and *Il17a*$^{-/-}$ mice (Supplementary Fig. 2). Our data thus suggest that IL-17A is a key factor in the homeostatic expansion of T_{reg} cells in visceral adipose tissue.

γδ T cells with specific V-gene rearrangements leave the thymus in concerted waves during neonatal development and seed

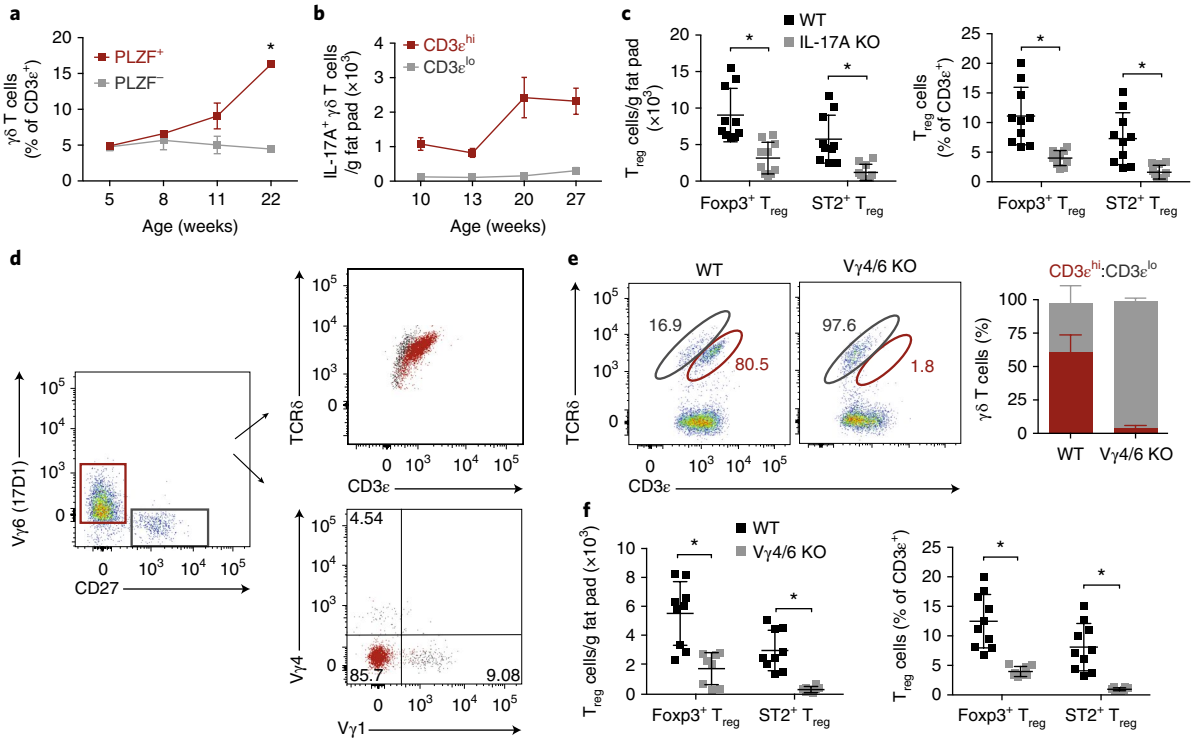

Fig. 5 | ST2$^+$ T_{reg} numbers depend on PLZF$^+$ γδ T cells and IL-17A. a, Frequency of PLZF$^+$ and PLZF$^-$ γδ T cells from eWAT at 5, 8, 11, and 22 weeks of age ($n = 5$ mice per time point). **b**, Numbers of GFP$^+$ CD3ε^{hi} and CD3ε^{lo} γδ T cells from eWAT of *Il17a*^{GFP} male mice at 10, 13, 20, and 27 weeks of age ($n = 5$ mice per time point). **c**, Numbers and frequency of ST2$^+$ and total T_{reg} cells from eWAT of 16-week-old males from WT and *Il17a*$^{-/-}$ mice ($n = 5$ mice, pooled). **d**, Representative flow cytometry of γδ T cells stained with anti-CD27, 17D1, anti-Vγ1, and anti-Vγ4 to characterize TCR usage. **e**, Representative flow cytometry plots of γδ T cells from WT and *Vg4/6*$^{-/-}$ eWAT (left) and quantification of CD3ε^{hi} and CD3ε^{lo} γδ frequencies (right) ($n = 5$ mice). **f**, Numbers and frequency of ST2$^+$ and total T_{reg} cells from eWAT of 16-week-old WT and *Vg4/6*$^{-/-}$ male mice ($n \geq 4$). Each symbol represents an individual mouse; small horizontal lines indicate the mean. NS, not significant ($P > 0.05$); *$P < 0.05$ (one-way ANOVA in **a**,**c**,**f**). Data are pooled across two experiments (mean ± s.e.m. in **a**–**c**,**f**) or representative of two experiments (**d**,**e**; mean ± s.e.m. in **e**).

tissues[29]. The innate-IL17A-producing subset is largely dominated by Vγ6$^+$ TCRs, although other IL-17A-producing Vγ4$^+$ cells can arise later. Because some PLZF$^+$ γδ T cells have been reported to bear the canonical Vγ6$^+$ TCR chain, we stained γδ T cells from adipose tissue with antibodies to determine TCR usage[30]. In adipose tissue from mice at 20 weeks of age, most CD3ε^{hi}PLZF$^+$CD27$^-$ γδ T cells were Vγ6$^+$, whereas CD3ε^{lo}PLZF$^-$CD27$^+$ γδ T cells expressed Vγ1$^+$ and Vγ4$^+$ TCR chains and composed a smaller fraction of the total adipose γδ T cells (Fig. 5d).

To deplete most of the PLZF$^+$ γδ T cells, we characterized adipose tissue from Vγ4- and Vγ6-deficient (*Vg4/6*$^{-/-}$) mice. We confirmed that the *Vg4/6*$^{-/-}$ mice had severely low numbers of PLZF$^+$CD3ε^{hi} γδ T cells in adipose tissue, whereas PLZF$^-$CD3ε^{lo} γδ T cells were still present (Fig. 5e). Next, we analyzed 20-week-old *Vg4/6*$^{-/-}$ mice and found that they, like *Il17a*$^{-/-}$ and *Tcrd*$^{-/-}$ mice, displayed significantly fewer total adipose Foxp3$^+$ and ST2$^+$ T_{reg} cells than did wild-type mice (Fig. 5f). When profiling other immune populations, we observed similar frequencies of ILC2s, but unexpectedly, the number of *i*NKT cells was significantly lower in *Vg4/6*$^{-/-}$ mice than in wild-type mice, thus suggesting that cross-talk may exist between PLZF$^+$ γδ T cells and *i*NKT cells in adipose tissue (Supplementary Fig. 2). Interestingly, the low frequencies of ST2$^+$ T_{reg} cells were not observed in the spleen and lung in *Il17a*$^{-/-}$ and *Vg4/6*$^{-/-}$ mice (Supplementary Fig. 2). In summary, these data uncover an important role of both IL-17A and PLZF$^+$ γδ T cells in age-dependent increases in adipose tissue T_{reg} cell numbers.

TNF and IL-17A induce IL-33 in adipose stromal cells. IL-33, a member of the IL-1 family of cytokines, is an important regulator of adipose ILC2 and T_{reg} cell homeostasis because both cell types express the cognate receptor, ST2 (refs [11,15,31–34]). Adipose T_{reg} cells have high expression of ST2, and engagement of the ST2 receptor by IL-33 results in T_{reg} proliferation[11,15]. We found that IL-33 protein increased with age in visceral adipose tissue, in a manner concomitant with T_{reg} and PLZF$^+$ γδ T cell accumulation (Fig. 6a). Because of the significantly lower T_{reg} numbers in *Tcrd*$^{-/-}$, *Il17a*$^{-/-}$, and *Vg4/6*$^{-/-}$ mice compared with wild-type mice, we asked whether γδ T cells might affect IL-33 in adipose tissue. Indeed, 20-week-old *Tcrd*$^{-/-}$ mice, compared with wild-type mice, showed significantly less in IL-33 protein in the adipose tissue but not the spleen (Fig. 6b). IL-2, a critical cytokine for T_{reg} maintenance in other peripheral organs, did not differ between wild-type and *Tcrd*$^{-/-}$ mice (Fig. 6b). IL-33 protein in adipose tissue was clearly less abundant in *Il17a*$^{-/-}$ and *Vg4/6*$^{-/-}$ mice than in wild-type mice (Fig. 6c). Interestingly, *Il17a*$^{-/-}$ mice had significantly less IL-33 protein and fewer ST2$^+$ T_{reg} cell numbers in visceral adipose tissue even at 11 weeks of age, thus suggesting that this phenotype manifests earlier in *Il17a*$^{-/-}$ mice than in wild-type mice (Supplementary Fig. 2). Together, these results suggest that IL-17A-producing PLZF$^+$ γδ T cells are necessary for age-induced increases IL-33 protein in visceral adipose tissue.

To assess the contribution of IL-17A-producing PLZF$^+$ γδ T cells to IL-33 concentrations, we sought to identify the IL-33-expressing cell type and, importantly, test whether it would respond to IL-17A. Flow cytometry of the adipose stromal compartment identified a substantial population of CD31$^+$ endothelial cells, as well as Pdpn$^+$ (gp38$^+$) stromal cells, among the nonhematopoietic (CD45$^-$) pool (Fig. 6d). These Pdpn$^+$ cells could further be segregated according to their expression of the surface marker

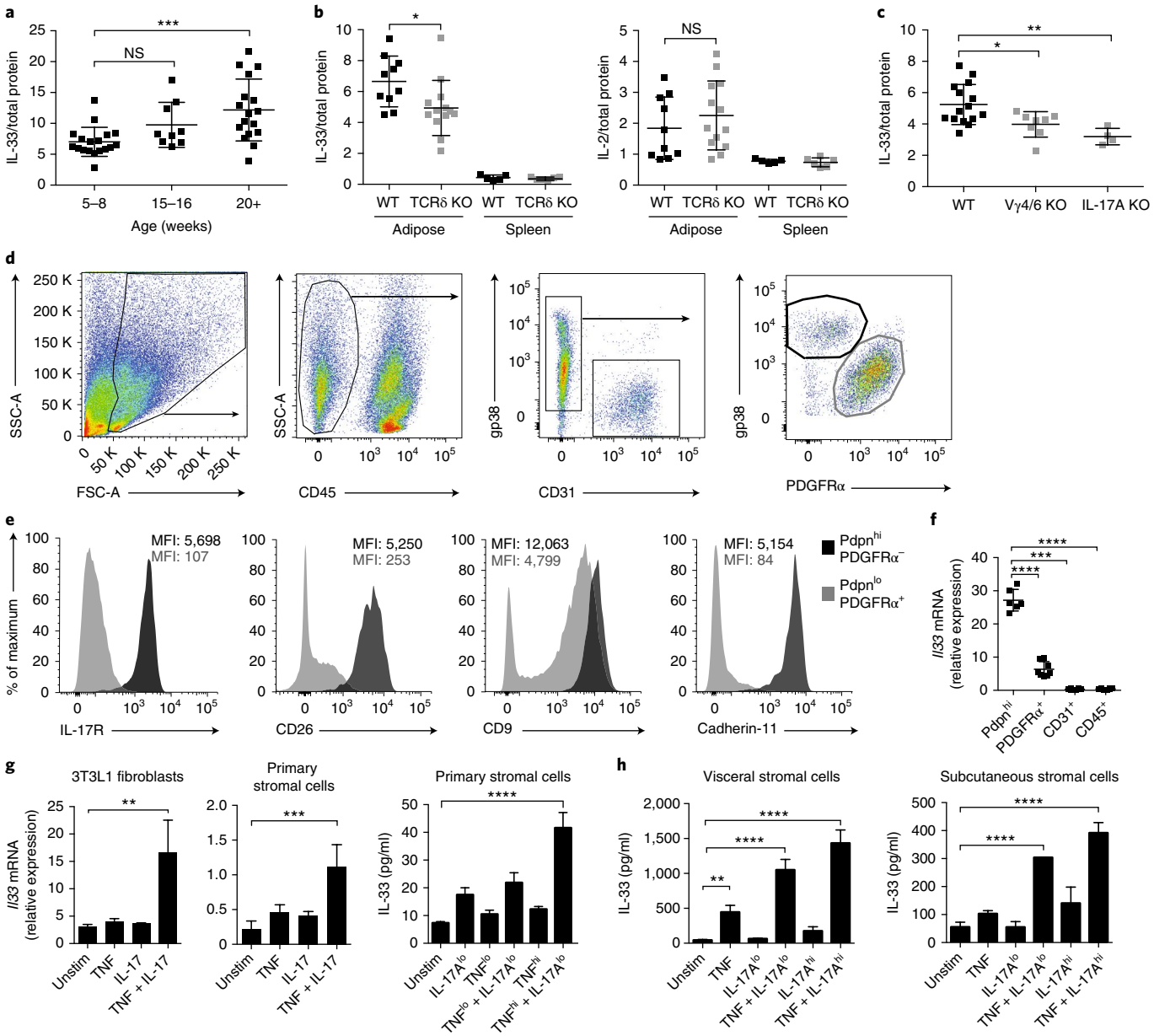

Fig. 6 | TNF and IL-17A induce IL-33 in adipose stromal cells. a, IL-33 protein from SVF eWAT lysates of WT male mice 5–8, 15–16, and 20+ weeks of age, determined by enzyme-linked immunosorbent assay (ELISA; $n = 4$ mice per time point) and normalized to total SVF protein. **b**, IL-33 (left) and IL-2 (right) protein from SVF eWAT and splenic lysates of 14-week-old WT and *Tcrd*$^{-/-}$ male mice ($n \geq 3$, pooled). **c**, IL-33 protein from SVF eWAT lysates of 16-week-old WT, *Vg4/6*$^{-/-}$, and *Il17a*$^{-/-}$ male mice ($n \geq 4$), normalized to total SVF protein. **d**, Representative flow cytometry plots for stromal cell subsets in the eWAT SVF in male WT mice. **e**, Cell-surface IL-17R, CD26, CD9, and Cdh11 MFI of CD45$^-$Pdpn^{hi}PDGFRα$^-$ and CD45$^-$Pdpn^{lo}PDGFRα$^+$ stromal cells. **f**, Quantitative real-time PCR for *Il33* mRNA normalized to *Tbp* mRNA from sorted Pdpn^{hi}, PDGFRα$^+$, CD31$^+$, and CD45$^+$ cells from WT mice ($n = 6$). **g**, 3T3L1 or primary adipose stromal cells derived from eWAT SVF were unstimulated (unstim) or stimulated with TNF^{lo} (0.1 ng/mL), TNF (1 ng/mL), IL-17A^{lo} (0.1 ng/mL), IL-17A (1 ng/mL), or TNF (1 ng/mL) + IL-17A (1 ng/mL) for 18 h. *Il33* transcript levels were measured with quantitative real-time PCR (left), and protein levels were measured with ELISA (right). **h**, Primary human stromal cells derived from visceral (Lonza) and subcutaneous (ATCC) adipose tissues were unstimulated (unstim) or stimulated with TNF^{lo} (0.1 ng/mL), TNF (1 ng/mL), IL-17A^{lo} (0.1 ng/mL), IL-17A (1 ng/mL), or TNF (1 ng/mL) + IL-17A (1 ng/mL) for 18 h. Cell lysates were collected, and IL-33 protein was measured with ELISA. In plots, each symbol represents an individual mouse; small horizontal lines indicate the mean. NS, not significant ($P > 0.05$); *$P < 0.05$; **$P < 0.01$; ***$P < 0.001$; ****$P < 0.0001$ (one-way ANOVA in **a**–**c**,**f**–**h**). Data are pooled across three experiments (**a**–**c**; mean ± s.e.m.) or representative of two experiments (**d**–**h**; mean ± s.e.m. in **f**–**h**).

platelet-derived growth factor receptor-alpha (PDGFRα) (Fig. 6d) as well as CD26, CD9, and Cdh11 (Fig. 6e). Staining for IL-17 receptor (IL-17R) to determine the subset that would respond to IL-17A identified Pdpn$^+$CD26$^+$PDGFRα$^-$Cdh11$^+$ stromal cells as the dominant IL-17R-expressing population in adipose tissue (Fig. 6e). Intriguingly, when we quantified *Il33* mRNA from sorted stromal cells, we found that Pdpn$^+$PDGFRα$^-$ cells, as compared with other cells in adipose tissue, highly expressed *Il33* (Fig. 6f). Our data highlight Pdpn$^+$CD26$^+$PDGFRα$^-$Cdh11$^+$ stromal cells as the main IL-33- and IL-17R-expressing cell type in visceral adipose tissue.

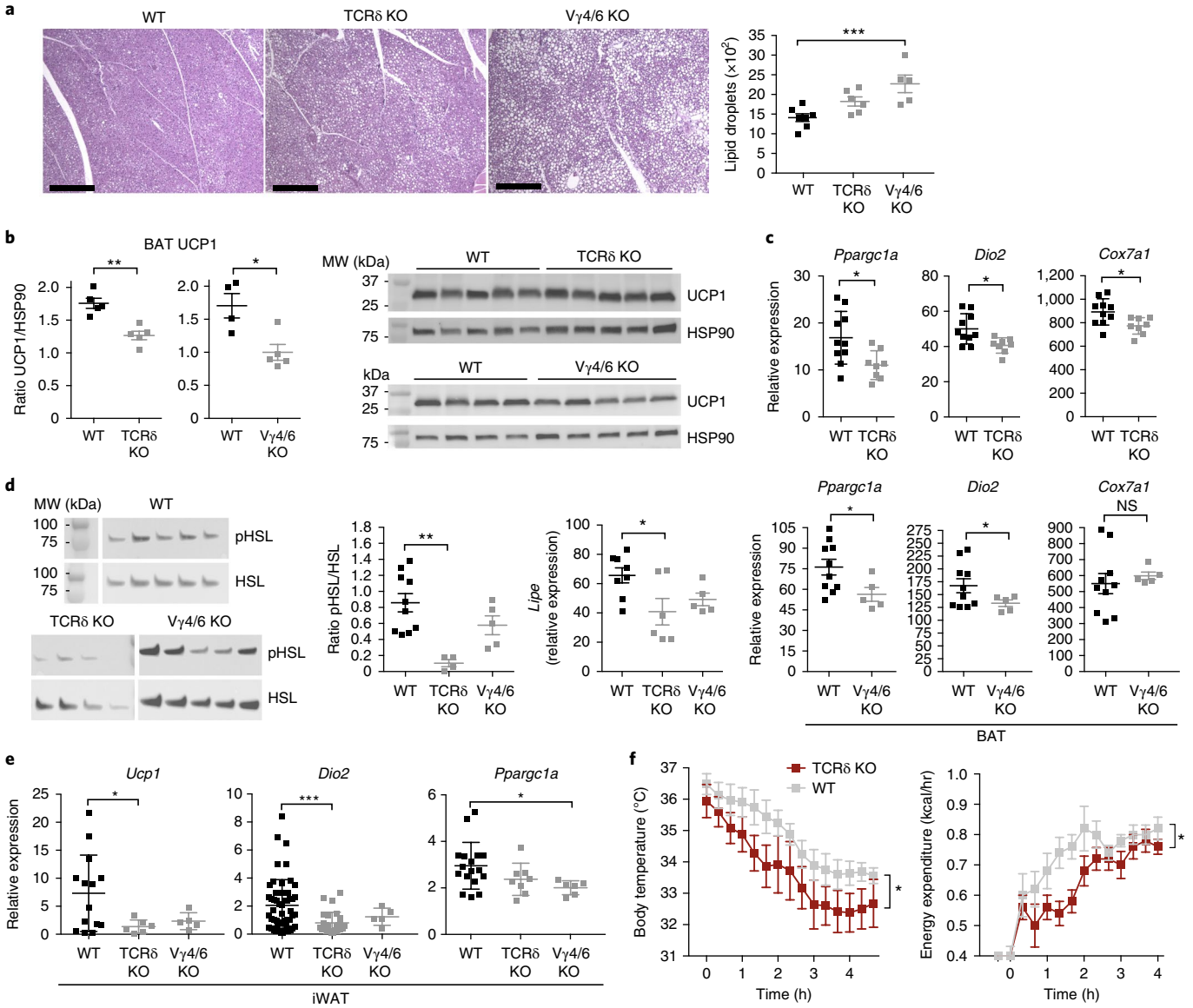

Fig. 7 | γδ T cells are important for adaptive thermogenesis after cold. a, Representative histology of hematoxylin- and eosin-stained BAT and lipid-droplet quantification from WT, *Tcrd*$^{-/-}$, and *Vg4/6*$^{-/-}$ mice after 6 h at 4 °C. Scale bars, 500 µm. **b**, Immunoblot analysis and densitometry quantification of UCP1 and HSP90 loading control in BAT of WT, *Tcrd*$^{-/-}$, and *Vg4/6*$^{-/-}$ mice after 6 h at 4 °C ($n = 5$ mice). MW, molecular weight. **c**, Quantitative real-time PCR of thermogenesis genes from WT and *Tcrd*$^{-/-}$ BAT (top), and WT and *Vg4/6*$^{-/-}$ BAT (bottom) after 6 h at 4 °C ($n \geq 5$ mice). **d**, Immunoblot analysis of phospo-HSL (pHSL) and HSL and quantitative real-time PCR of *Lipe* (also known as *Hsl*) from iWAT of WT, *Tcrd*$^{-/-}$, and *Vg4/6*$^{-/-}$ mice after 6 h at 4 °C ($n \geq 5$ mice). **e**, Quantitative real-time PCR of thermogenesis genes from WT, *Tcrd*$^{-/-}$, and *Vg4/6*$^{-/-}$ iWAT after 6 h at 4 °C ($n \geq 5$ mice). **f**, Body temperature (left) and energy expenditure (right) in WT and *Tcrd*$^{-/-}$ male mice from 30 °C to 4 °C ($n = 5$ per group). Each symbol represents an individual mouse; small horizontal lines indicate the mean. Gene expression normalized to *Tbp*. Immunoblots have been cropped to show relevant proteins. NS, not significant ($P > 0.05$); *$P < 0.05$; **$P < 0.01$; ***$P < 0.001$ (metabolic variable adjusted for differences in body composition by analysis of covariance (ANCOVA) in **g**; one-way ANOVA in **a**,**e**,**f**; two-tailed Student's *t* test in **b**,**c**). Data are representative of two experiments (**a**–**f**; mean ± s.e.m. in **a**–**g**).

In addition to amplifying inflammation, IL-17A plays important homeostatic and antimicrobial roles at mucosal sites[35]. However, its effects on adipose tissue stromal cells (fibroblasts and adipocytes), as well as other resident immune cells, are less appreciated[36]. Because *Il17a*$^{-/-}$ mice exhibited severely low T_{reg} cell numbers and IL-33 protein, we asked whether IL-17A might be sufficient to induce IL-33 expression in adipose stromal cells. Using 3T3L1 preadipocytes and fresh primary adipose stromal cells, we found that IL-17A stimulated increases in *Il33* mRNA and IL-33 protein, but the presence of both TNF and IL-17A synergistically induced high expression of IL-33 (Fig. 6g). Moreover, this stimulation was specific to the combination of TNF and IL-17A, because neither IFN-γ nor IL-1β increased IL-33 to the same extent (Supplementary Fig. 3).

We next injected purified recombinant TNF and IL-17A into mice and found that, after injection, *Il33* mRNA increased in adipose tissue (Supplementary Fig. 3). Mechanistically, TNF and IL-17A expanded IL-33-expressing Pdpn$^+$ stromal cells and upregulated *Il33* mRNA within the PDGFRα$^+$ population (Supplementary Fig. 3). Although Pdpn$^+$ stromal cells expressed the highest amounts of IL-33 at steady state, in vivo, both Pdpn$^+$ and PDGFRα$^+$ stromal subsets appeared to contribute to endogenous IL-33 expression in visceral adipose tissue and to be affected by TNF and IL-17A.

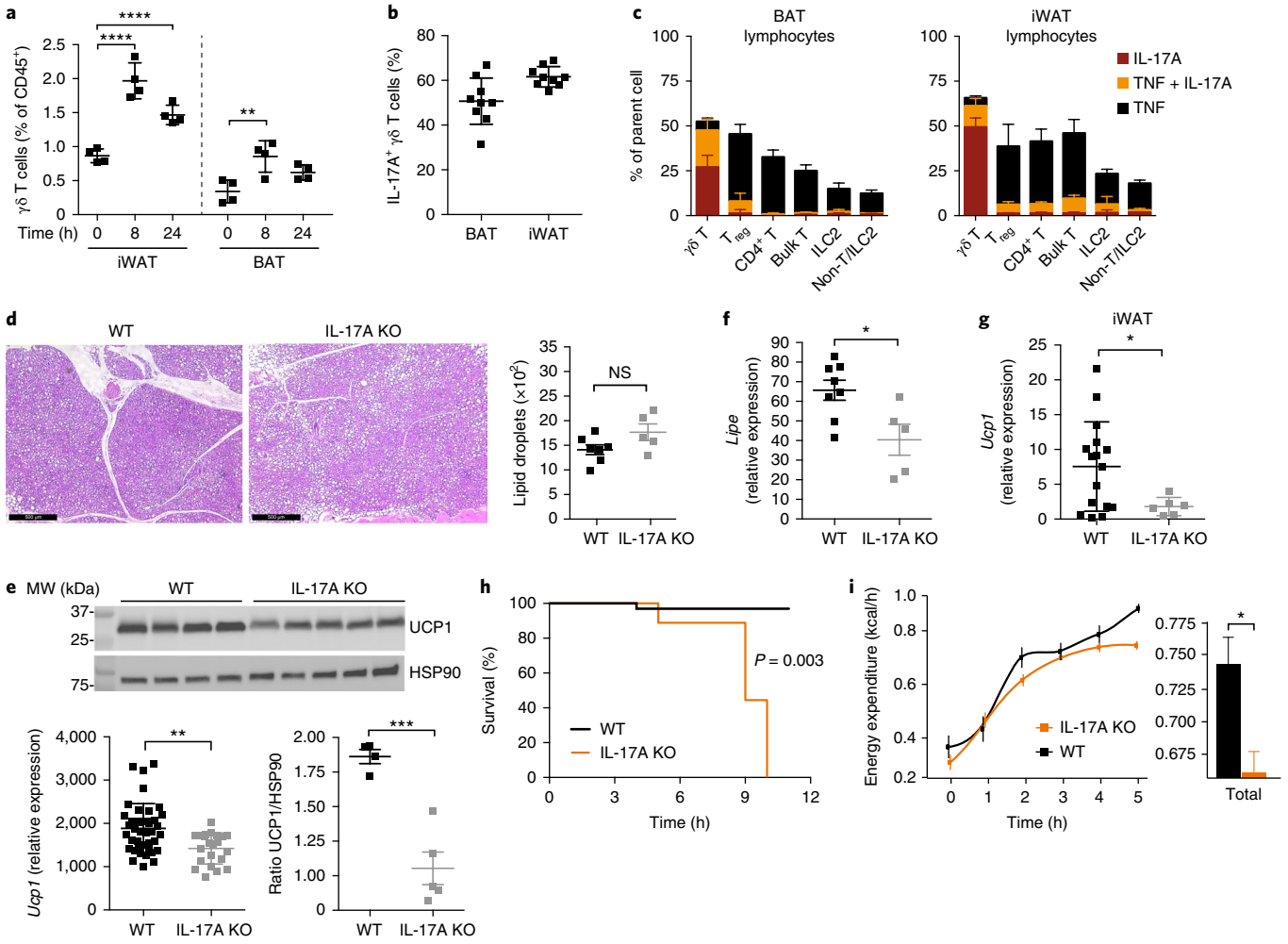

Fig. 8 | IL-17A promotes thermogenic responses in brown and inguinal adipose tissue. a, Frequency of γδ T cells of CD45⁺ cells in BAT and iWAT 0, 8, and 24 h at 4 °C ($n = 4$ mice). **b**, Frequency of IL-17A-producing γδ T cells from BAT and iWAT after 5-h stimulation with PMA and ionomycin ($n = 10$ mice). **c**, Frequency of immune cells from BAT and iWAT that produce TNF, IL-17A, or TNF + IL-17A after 4-h stimulation with PMA and ionomycin at 4 °C ($n = 5$ mice). **d**, Representative histology of hematoxylin- and eosin-stained BAT and lipid-droplet quantification from WT and *Il17a*$^{-/-}$ mice after 6 h at 4 °C. Scale bars, 500 µm. **e**, Quantitative real-time PCR of *Ucp1* (left) and immunoblot analysis of UCP1 and HSP90 loading control (right) in BAT tissue obtained from WT and *Il17a*$^{-/-}$ mice ($n \geq 5$) after 6 h at 4 °C. **f**, Quantitative real-time PCR of *Lipe* (also known as *Hsl*) from WT and *Il17a*$^{-/-}$ iWAT after 6 h at 4 °C ($n \geq 5$ mice). **g**, Quantitative real-time PCR of *Ucp1* from WT and *Il17a*$^{-/-}$ iWAT after 6 h at 4 °C ($n \geq 5$ mice). **h**, WT and *Il17a*$^{-/-}$ mice were gradually shifted from 30 °C to 4 °C at a continuous rate and monitored for survival. Mice ($n = 5$) were rescued when body temperature dropped to <28 °C. **i**, Energy expenditure measured between WT and *Il17a*$^{-/-}$ male mice ($n = 5$). Each symbol represents an individual mouse; small horizontal lines indicate the mean. Gene expression was normalized to that of *Tbp*. Immunoblots have been cropped to show relevant proteins. NS, not significant ($P > 0.05$); *$P < 0.05$; **$P < 0.01$; ***$P < 0.001$; ****$P < 0.0001$ (metabolic variable adjusted for differences in body composition by ANCOVA in **h**,**i**; one-way ANOVA in **a**; Two-tailed Student's *t* test in **d**–**g**; log-rank Mantel–Cox test in **h**). Data are representative of two experiments (**a**–**g**; mean ± s.e.m. in **a**–**g**).

To assess why mice deficient in γδ T cells or IL-17A exhibited low IL-33 expression in adipose tissue, we quantified the numbers and IL-33 expression of stromal populations from wild-type, *Tcrd*$^{-/-}$, *Vg4/6*$^{-/-}$, and *Il17a*$^{-/-}$ mice. We found that both the Pdpn⁺ and PDGFRα⁺ stromal-subset numbers were markedly low in *Tcrd*$^{-/-}$, *Vg4/6*$^{-/-}$, and *Il17a*$^{-/-}$ mice, whereas IL-33 expression within stromal cells showed no significant differences (Supplementary Fig. 4). Our data suggest that in γδ-deficient and IL-17A-deficient animals, the low IL-33 expression is largely a result of low numbers of IL-33-expressing or IL-33-producing Pdpn⁺ and PDGFRα⁺ cells, respectively, but is less dependent on lower *Il33* mRNA within stromal populations.

Recent reports have demonstrated IL-33 expression in human adipocytes and endothelial cells[37,38] and have indicated that human omental T_{reg} cells express ST2 (ref. [11]). We asked whether this newly defined IL-17A–TNF–IL-33 axis might exist in human adipose tissue. In human primary preadipocytes from both visceral and subcutaneous adipose depots, stimulation with TNF and IL-17A greatly enhanced expression of IL-33 (Fig. 6h). Together, our results indicate that TNF and IL-17A produced by PLZF⁺ γδ T cells promote IL-33 within the stromal compartment in adipose tissue.

γδ T cells and IL-17A regulate body temperature. Beyond its role in adipose immune regulation, IL-33 is important in thermogenesis, the metabolic adaptation to cold temperatures[17,18]. When we extended our analysis to brown adipose tissue (BAT) and inguinal white adipose tissue (iWAT), depots important for increasing body temperature, we found that IL-33 protein was significantly less abundant in the BAT in *Tcrd*$^{-/-}$ and *Vg4/6*$^{-/-}$ mice than in wild-type mice (Supplementary Fig. 5). Although the protein levels were not different in iWAT, *Il33* mRNA was less abundant in *Tcrd*$^{-/-}$ and *Vg4/6*$^{-/-}$ mice than in wild-type mice (Supplementary Fig. 5), thus raising the possibility that mice lacking γδ T cells might exhibit defects in body-temperature regulation.

In support of this possibility, histological sections of BAT from cold-challenged mice showed that *Tcrd*$^{-/-}$ and *Vg4/6*$^{-/-}$ mice, compared with their wild-type littermates, contained more lipids in brown adipocytes (Fig. 7a). Importantly, *Tcrd*$^{-/-}$ and *Vg4/6*$^{-/-}$ mice, compared with wild-type mice, had less UCP1 protein in BAT, and lower expression of thermogenic genes, including *Ppargc1a*, *Dio2*, and *Cox7a1*, after cold challenge (Fig. 7b,c). Notably, when we evaluated iWAT after cold challenge, we found that *Tcrd*$^{-/-}$ and *Vg4/6*$^{-/-}$ mice, compared with wild-type mice, were unable to burn lipids, as evidenced by gross anatomy (Supplementary Fig. 5), and had lower expression and activation of hormone-sensitive lipase (HSL), a critical lipolytic enzyme (Fig. 7d). Like the BAT, the iWAT depot from *Tcrd*$^{-/-}$ and *Vg4/6*$^{-/-}$ mice, compared with wild-type mice, after cold challenge showed lower expression of thermogenic genes (Fig. 7e), thus suggesting that mice deficient in γδ T cells are unable to upregulate adaptive thermogenesis in BAT and iWAT.

To determine whether these local adipose defects had physiological consequences, we measured body temperature and energy expenditure through indirect calorimetry. The body temperature of *Tcrd*$^{-/-}$ mice, compared with that of wild-type mice, decreased significantly more rapidly in the cold, and the knockout mice correspondingly were unable to increase energy expenditure (Fig. 7f). Of note, when challenged with the β-adrenergic agonist CL-316 243, which maximally activates BAT thermogenesis, *Tcrd*$^{-/-}$ mice did not show a defect in their ability to expend energy as heat, thereby suggesting that β-adrenergic signaling is downstream of γδ T cell control (Supplementary Fig. 5). Thus, mice deficient in γδ T cells are unable to engage nonshivering thermogenesis in response to cold, in part because of an inability to upregulate factors important for turning on the thermogenic program in BAT and iWAT.

To better understand how γδ T cells promote thermogenic responses, we quantified the frequencies and cytokine profiles of γδ T cells in BAT and iWAT after cold challenge. We found that 8 h after cold challenge, γδ T cells significantly increased in frequency in both BAT and iWAT and remained elevated at 24 h (Fig. 8a). Despite their increased frequency, the number of γδ T cells did not change, thus suggesting a decline in other immune populations with cold (Supplementary Fig. 6). When γδ T cells were stimulated with the phorbol ester PMA and ionomycin, more than 40% produced IL-17A in BAT and iWAT (Fig. 8b). In contrast, other immune populations produced little IL-17A, thus highlighting the role of γδ T cells as the dominant source of IL-17A in both depots (Fig. 8c). γδ T cells thus make up a larger percentage of immune cells after cold challenge and are a major source of IL-17A in situ.

Because γδ T cells produce IL-17A in BAT and iWAT, we hypothesized that IL-17A might be an important regulator of the thermogenic phenotype observed. Indeed, like *Tcrd*$^{-/-}$ and *Vg4/6*$^{-/-}$ mice, *Il17a*$^{-/-}$ mice exhibited more lipid droplets in BAT than did wild-type mice (Fig. 8d) and did not upregulate BAT UCP1 (Fig. 8e) after cold exposure. Moreover, defects in lipolysis were observed in the iWAT in *Il17a*$^{-/-}$ mice (Fig. 8f), and a similar inability of *Il17a*$^{-/-}$ mice to upregulate *Ucp1* in iWAT was measured (Fig. 8g). *Il17a*$^{-/-}$ mice, compared with wild-type mice, showed lower expression of other thermogenic genes in both BAT and iWAT (Supplementary Fig. 6). Strikingly, when WT and *Il17a*$^{-/-}$ mice were placed in metabolic cages for indirect calorimetry assessment, all of the *Il17a*$^{-/-}$ mice had to be rescued from death 5–12 h after cold challenge, because of their inability to increase energy expenditure (Fig. 8h,l). This inability was evidenced by the lack of increase in body temperature 5 h after cold challenge (Supplementary Fig. 6). Interestingly, *Il17a*$^{-/-}$ mice also showed abnormal circadian control of body temperature and the respiratory exchange ratio (Supplementary Fig. 6). Together, these data support a critical role for IL-17A in body-temperature regulation.

To understand the mechanism underlying thermogenic control by γδ T cells and IL-17A, we first quantified the gene expression of thermogenic enzymes and receptors (Supplementary Fig. 7). Interestingly, *Adrb3* mRNA decreased across all genotypes in iWAT at thermoneutrality and after cold. Expression of *Lipe* and *Pnpla2*, two key genes for lipolysis, also significantly decreased, thus suggesting that mice lacking γδ T cells or IL-17A were relatively less sensitive to catecholamine stimulation for lipolysis induction. Second, stimulation with TNF and IL-17A synergistically upregulated thermogenic genes including *Ucp1*, *Dio2*, *Cidea*, and *Il33* in brown adipocyte cultures (Supplementary Fig. 8). Stimulation with IL-33 itself did not induce the same increases in gene expression, thus suggesting that TNF and IL-17A can induce a thermogenic program in BAT independently of IL-33 (Supplementary Fig. 8). In iWAT, TNF and IL-17A injections in vivo were sufficient to induce *Ucp1*, *Ppargc1a*, and *Dio2* in sorted Pdpn$^+$ stromal cells but not PDGFRα$^+$ cells (Supplementary Fig. 8). Finally, in BAT and iWAT in wild-type, *Tcrd*$^{-/-}$ and *Vγ4/6*$^{-/-}$ mice, we quantified immune cells known to be important for thermogenic responses (Supplementary Fig. 8). There were no differences observed in the ILC2, eosinophil, *i*NKT, and T_{reg} frequencies between wild-type and *Tcrd*$^{-/-}$ mice in both depots, thus suggesting that the thermogenic defects seen in γδ T cell–deficient mice were independent of other immune populations. Together, our data suggest that γδ T cells promote thermogenic responses directly through the cytokines that they produce, namely TNF and IL-17A, and indirectly through maintenance of catecholamine sensitivity.

Discussion

The role of γδ T cells as guardians against pathogens at barrier sites has been well documented. However, the physiological roles of γδ T cells at steady state and in nonbarrier tissues are less appreciated. We uncovered a new biological axis in which PLZF$^+$ IL-17A-producing γδ T cells cross-talk with adipose stromal cells and consequently regulate IL-33 abundance and exert downstream effects on T_{reg} cell accumulation and thermoregulation. Post-translational processing tightly controls the levels of IL-33 (ref. [39]), but the upstream mechanisms that control its transcription have been less studied. In addition, the main cell type that produces IL-33 in mouse adipose tissue had been a matter of debate. Our studies reveal Pdpn$^+$ and PDGFRα$^+$ cells to be IL-17A-responsive stromal cells in visceral adipose tissue. Moreover, TNF and IL-17A synergistically increase the cell numbers and *Il33* expression, respectively, of Pdpn$^+$ and PDGFRα$^+$ cells, thereby modulating IL-33 abundance in situ. These findings highlight an important homeostatic role of IL-17A in adipose tissue, a function independent of its antimicrobial role.

Such effects mediated by γδ T cells are also intriguing given the previously defined roles of *i*NKT cells that also regulate T_{reg} cell homeostasis[3,7]. We suggest that, whereas *i*NKT cells play a key role in regulating T_{reg} numbers and function in young mice via IL-2, PLZF$^+$ γδ T cells play a key role in adult mice via IL-33 when *i*NKT cell numbers decline. Despite their important roles as regulators of type 2 immunity in young mice, ILC2s and *i*NKT cells decrease with age, while a new wave of immune cells composed of γδ T cells and T_{reg} cells expand. This temporal regulation of adipose lymphocytes may ensure redundancy in the molecular pathways that maintain healthy adipose tissue, as is critical for local and systemic metabolic homeostasis.

In addition, we discovered that γδ T cells and the cytokine IL-17A are critical regulators of thermogenesis, a distinctive function of adipose tissue. Deficiencies in γδ T cells and IL-17A dramatically affect the ability of mice to survive after cold challenge and robustly induce UCP1-dependent thermogenic responses. Remarkably, *i*NKT cells and PLZF$^+$ γδ T cells in adipose tissue regulate thermogenesis through FGF-21 and IL-17A, respectively[3,7]. These roles of *i*NKT cells and γδ T cells in regulating both T_{reg} cells and thermogenesis through complementary mechanisms underscores the remarkable importance of these innate T cell populations in adipose tissue. Our work opens a new dimension in adipose biology, whereby the dynamic cross-talk between innate lymphocytes and tissue-specific stromal cells dictates local immune composition and systemic energy expenditure.

Methods

Methods, including statements of data availability and any associated accession codes and references, are available at https://doi.org/10.1038/s41590-018-0094-2.

Received: 14 August 2017; Accepted: 16 March 2018;
Published online: 18 April 2018

References

1. Brestoff, J. R. & Artis, D. Immune regulation of metabolic homeostasis in health and disease. *Cell* **161**, 146–160 (2015).
2. Kohlgruber, A. & Lynch, L. Adipose tissue inflammation in the pathogenesis of type 2 diabetes. *Curr. Diab. Rep.* **15**, 92 (2015).
3. Lynch, L. et al. Regulatory *i*NKT cells lack expression of the transcription factor PLZF and control the homeostasis of T_{reg} cells and macrophages in adipose tissue. *Nat. Immunol.* **16**, 85–95 (2015).
4. Lynch, L. et al. Adipose tissue invariant NKT cells protect against diet-induced obesity and metabolic disorder through regulatory cytokine production. *Immunity* **37**, 574–587 (2012).
5. Molofsky, A. B. et al. Innate lymphoid type 2 cells sustain visceral adipose tissue eosinophils and alternatively activated macrophages. *J. Exp. Med.* **210**, 535–549 (2013).
6. Nussbaum, J. C. et al. Type 2 innate lymphoid cells control eosinophil homeostasis. *Nature* **502**, 245–248 (2013).
7. Lynch, L. et al. *i*NKT cells induce FGF21 for thermogenesis and are required for maximal weight loss in GLP1 therapy. *Cell Metab.* **24**, 510–519 (2016).
8. Brestoff, J. R. et al. Group 2 innate lymphoid cells promote beiging of white adipose tissue and limit obesity. *Nature* **519**, 242–246 (2015).
9. Feuerer, M. et al. Lean, but not obese, fat is enriched for a unique population of regulatory T cells that affect metabolic parameters. *Nat. Med.* **15**, 930–939 (2009).
10. Cipolletta, D. et al. PPAR-γ is a major driver of the accumulation and phenotype of adipose tissue T_{reg} cells. *Nature* **486**, 549–553 (2012).
11. Vasanthakumar, A. et al. The transcriptional regulators IRF4, BATF and IL-33 orchestrate development and maintenance of adipose tissue-resident regulatory T cells. *Nat. Immunol.* **16**, 276–285 (2015).
12. Bapat, S. P. et al. Depletion of fat-resident T_{reg} cells prevents age-associated insulin resistance. *Nature* **528**, 137–141 (2015).
13. Cipolletta, D. Adipose tissue-resident regulatory T cells: phenotypic specialization, functions and therapeutic potential. *Immunology* **142**, 517–525 (2014).
14. Panduro, M., Benoist, C. & Mathis, D. Tissue Tregs. *Annu. Rev. Immunol.* **34**, 609–633 (2016).
15. Kolodin, D. et al. Antigen- and cytokine-driven accumulation of regulatory T cells in visceral adipose tissue of lean mice. *Cell Metab.* **21**, 543–557 (2015).
16. Molofsky, A. B. et al. Interleukin-33 and interferon-γ counter-regulate group 2 innate lymphoid cell activation during immune perturbation. *Immunity* **43**, 161–174 (2015).
17. Mathis, D. IL-33, imprimatur of adipocyte thermogenesis. *Cell* **166**, 794–795 (2016).
18. Odegaard, J. I. et al. Perinatal licensing of thermogenesis by IL-33 and ST2. *Cell* **166**, 841–854 (2016).
19. Lee, M.-W. et al. Activated type 2 innate lymphoid cells regulate beige fat biogenesis. *Cell* **160**, 74–87 (2015).
20. Jackson-Jones, L. H. et al. Fat-associated lymphoid clusters control local IgM secretion during pleural infection and lung inflammation. *Nat. Commun.* **7**, 12651 (2016).
21. Pichery, M. et al. Endogenous IL-33 is highly expressed in mouse epithelial barrier tissues, lymphoid organs, brain, embryos, and inflamed tissues: in situ analysis using a novel Il-33-LacZ gene trap reporter strain. *J. Immunol.* **188**, 3488–3495 (2012).
22. Paget, C. et al. CD3bright signals on γδ T cells identify IL-17A-producing Vγ6Vδ1$^+$ T cells. *Immunol. Cell Biol.* **93**, 198–212 (2015).
23. Ribot, J. C. et al. CD27 is a thymic determinant of the balance between interferon-γ- and interleukin 17-producing γδ T cell subsets. *Nat. Immunol.* **10**, 427–436 (2009).
24. Kreslavsky, T. et al. TCR-inducible PLZF transcription factor required for innate phenotype of a subset of γδ T cells with restricted TCR diversity. *Proc. Natl Acad. Sci. USA* **106**, 12453–12458 (2009).
25. Lu, Y., Cao, X., Zhang, X. & Kovalovsky, D. PLZF controls the development of fetal-derived IL-17$^+$Vγ6$^+$ γδ T cells. *J. Immunol.* **195**, 4273–4281 (2015).
26. Savage, A. K. et al. The transcription factor PLZF directs the effector program of the NKT cell lineage. *Immunity* **29**, 391–403 (2008).
27. Alonzo, E. S. & Sant'Angelo, D. B. Development of PLZF-expressing innate T cells. *Curr. Opin. Immunol.* **23**, 220–227 (2011).
28. Vantourout, P. & Hayday, A. Six-of-the-best: unique contributions of γδ T cells to immunology. *Nat. Rev. Immunol.* **13**, 88–100 (2013).
29. Wei, Y.-L. et al. A highly focused antigen receptor repertoire characterizes γδ T cells that are poised to make IL-17 rapidly in naive animals. *Front. Immunol.* **6**, 118 (2015).
30. Roark, C. L. et al. Subset-specific, uniform activation among Vγ6/Vδ1$^+$ γδ T cells elicited by inflammation. *J. Leukoc. Biol.* **75**, 68–75 (2004).
31. Van Dyken, S. J. et al. Chitin activates parallel immune modules that direct distinct inflammatory responses via innate lymphoid type 2 and γδ T cells. *Immunity* **40**, 414–424 (2014).
32. Vannella, K. M. et al. Combinatorial targeting of TSLP, IL-25, and IL-33 in type 2 cytokine-driven inflammation and fibrosis. *Sci. Transl. Med.* **8**, 337ra65 (2016).
33. Schiering, C. et al. The alarmin IL-33 promotes regulatory T-cell function in the intestine. *Nature* **513**, 564–568 (2014).
34. Kuswanto, W. et al. Poor repair of skeletal muscle in aging mice reflects a defect in local, interleukin-33-dependent accumulation of regulatory T cells. *Immunity* **44**, 355–367 (2016).
35. Hepworth, M. R. Innate lymphoid cell regulation: meeting the long-lost cousin. *Trends Immunol.* **38**, 873–874 (2017).
36. Zúñiga, L. A. et al. IL-17 regulates adipogenesis, glucose homeostasis, and obesity. *J. Immunol.* **185**, 6947–6959 (2010).
37. Wood, I. S., Wang, B. & Trayhurn, P. IL-33, a recently identified interleukin-1 gene family member, is expressed in human adipocytes. *Biochem. Biophys. Res. Commun.* **384**, 105–109 (2009).
38. Zeyda, M. et al. Severe obesity increases adipose tissue expression of interleukin-33 and its receptor ST2, both predominantly detectable in endothelial cells of human adipose tissue. *Int. J. Obes. (Lond.)* **37**, 658–665 (2013).
39. Martin, N. T. & Martin, M. U. Interleukin 33 is a guardian of barriers and a local alarmin. *Nat. Immunol.* **17**, 122–131 (2016).

Acknowledgements

We thank A.T. Chicoine, flow cytometry core manager at the Human Immunology Center at BWH, for flow cytometry sorting. We thank D. Sant'Angelo (Rutgers Cancer Institute) for providing *Zbtb16*$^{-/-}$ mice and R. O'Brien (National Jewish Health) for providing *Vg4/6*$^{-/-}$- mice. Supported by NIH grant R01 AI11304603 (to M.B.B.), ERC Starting Grant 679173 (to L.L.), the National Health and Medical Research Council of Australia (1013667), an Australian Research Council Future Fellowship (FT140100278 for A.P.U.) and a National Health and Medical Research Council of Australia Senior Principal Research Fellowship (1117766 for D.I.G.).

Author contributions

A.C.K., L.L., and M.B.B. conceived and designed the experiments, and wrote the manuscript. A.C.K., N.M.L., L.L., H.N.N., M.S., T.P., and D.D. performed the experiments. S.T.G.-O. and T.S. performed the RNA-seq analysis. A.S.B. and A.I.M. provided advice and performed the CLAMS experiments. A.T. provided human bariatric patient samples. Parabiosis experiments were performed in the laboratory of U.v.A. H.-F.K., A.P.U. and D.I.G provided critical insight into the TCR chain usage of PLZF$^+$ γδ T cells. M.B.B., N.M.L., and L.L. critically reviewed the manuscript.

Competing interests

M.B.B. is a consultant to Roche.

Additional information

Supplementary information is available for this paper at https://doi.org/10.1038/s41590-018-0094-2.

Reprints and permissions information is available at www.nature.com/reprints.

Correspondence and requests for materials should be addressed to M.B.B. or L.L.

Publisher's note: Springer Nature remains neutral with regard to jurisdictional claims in published maps and institutional affiliations.

Methods

Mice. C57BL/6J (WT), *Il17a*$^{-/-}$, *Tcrd*$^{-/-}$, and *Il17a*^{GFP} mice were purchased from Jackson Laboratory. Littermates were bred and maintained in specific-pathogen-free animal facilities at Brigham and Women's Center for Comparative Medicine. In almost all experiments, male mice of specified ages were used. PLZF reporter mice (*Zbtb16*^{GFP} mice) and *Zbtb16*$^{-/-}$ were generated in the laboratory of D. Sant'Angelo as previously described[3,40]. *Vgamma4/6*$^{-/-}$ (*Vg4/6*$^{-/-}$) mice were a kind gift from R. O'Brien[30]. All studies were executed by following the relevant ethical regulations detailed in animal-use protocols. All animal work and protocols were approved by, and were in compliance with the guidelines of, the Institutional Animal Care and Use Committee of Brigham and Women's Hospital and Harvard Medical School.

Parabiosis. Parabiosis studies were conducted as previously described[41]. CD45.1$^+$ and CD45.2$^+$ mice were first anesthetized with ketamine (100 mg/kg body weight) and xylazine (10 mg/kg body weight). After mice were shaved, a linear incision was made from the scapulae to the lower abdomen on opposing sides of each member of the pair. Mice were placed side by side, and skin edges were sewn together. Each pair was housed singly, with food placed on the floor of the cage for the first week during recovery. Parabiotic mice were kept together for 2–3 weeks. Chimerism in the blood and tissues was defined for gated lymphocytes or lymphocyte subsets as the percentage of CD45.1$^+$ cells over the percentage of CD45.1$^+$ cells plus CD45.2$^+$ cells in CD45.2$^+$ mice, and as the percentage of CD45.2$^+$ cells over the percentage of CD45.2$^+$ cells plus CD45.1$^+$ cells in CD45.1$^+$ mice.

Comprehensive Lab Animal Monitoring System. Indirect calorimetry experiments were performed with a Comprehensive Lab Animal Monitoring System (CLAMS, Columbus Instruments) essentially as previously described[42]. Mice were surgically implanted with intraperitoneal wireless temperature transmitters. After recovery, mice were housed in the CLAMS and maintained at thermoneutrality for 3 d. To observe the response to adrenergic agonist versus the effects of injection alone, we first injected mice housed at thermoneutrality with a control solution of sterile saline (200 µl) and monitored them for 3 h. The animals were then injected (1 mg/kg) with the selective β3-adrenergic receptor agonist CL316,243 (Sigma) and monitored as indicated. For the 4 °C cold challenge, mice were gradually shifted from 30 °C to 4 °C at a continuous rate over 3 h. For each experimental condition, metabolic variables were adjusted for differences in body composition by ANCOVA in the R programming language with a custom package for indirect calorimetry experiments (CalR).

Tissue digestion. Adipose tissue was carefully excised, minced, and digested with 1 mg/mL collagenase type 2 (Worthington LS004188) in RPMI (Life Technologies) for 25 min at 37 °C, with shaking. Cells were passed through a 70-µm cell strainer, washed, and centrifuged for 5 min at 300 *g* to pellet the stromal-vascular fraction (SVF) from floating mature adipocytes. For the preparation of single-cell suspensions of the liver, the organ was perfused via the portal vein with 10 mL PBS and mashed through a 70-µm cell strainer. Liver samples underwent enrichment for lymphocytes by centrifugation with a Percoll gradient. Spleens were strained through a 70-µm cell strainer and spun. Pellets from all tissues were subjected to red blood cell lysis and subsequently resuspended in flow cytometry buffer (2% FBS and 0.02% NaN_3 in phenol-free DMEM) for further staining.

Flow cytometry and cell sorting. Single-cell suspensions were incubated with Fc-receptor-blocking antibody (14-0161-82; eBioscience) before being stained on ice. Dead cells were excluded with a live/dead Zombie Aqua stain (BioLegend). For intracellular transcription-factor staining, cells were fixed and permeabilized with eBioscience Transcription Factor Fix/Perm Buffer. Mouse antibodies were as follows. Anti-CD45 (30-F11), anti-CD45.1 (A20), anti-CD45.2 (104), anti-CD27 (LG.3A10), anti-CD69 (FN50), anti-CD44 (BJ18), anti-CD127 (A019D5), anti-CD4 (RM4-5), anti-CD8α (53-6.7), anti-TCRβ (H57-597), anti-KLRG1 (2F1/KLRG1), anti-pdpn (8.1.1), anti-CD26 (H194-112FC), and anti-CD31 (390) were purchased from BioLegend. Anti-Ter119 (TER-119), anti-F4/80 (BM8), anti-CD19 (ID3), anti-γδ TCR (GL3), anti-CD3e (500A2), anti-PLZF (Mags.21F7), anti-Foxp3 (FJK-16s), anti-ST2 (RMST2-2), anti-T-bet (4B10), anti-RORγt (B2D), anti-TNF (MP6-XT22), anti-IL-17A (17B7), anti-IFN-γ (XMB1.2), anti-PDGFRα (APA5), anti-IL-17RA (PAJ-17R), and streptavidin-APC (Cat 17-4317-82) were purchased from eBioscience. To stain for Vγ6$^+$ cells, we used GL3 (anti-TCRγδ) and 17D1 (anti-Vγ5 Vδ1) antibodies as previously described[30]. Anti-Vγ4 (UC3-10A6) was purchased from BD Pharmingen. Biotinylated anti-Cad11 was generated in house. Mouse PBS-57-loaded CD1d tetramers were from the NIH tetramer facility. Human antibodies were as follows. Anti-TCR Vδ1 (REA173) and anti-TCR Vδ2 (123R3) were purchased from Miltenyi Biotec. Anti-CD3 (UCHT1) was purchased from BioLegend. Anti-TCR Vδ3 was custom made in Labpan (Europe). After being stained, cells were passed through a 70-µm filter, and data were acquired on a BD FACSAria Fusion, BD Fortessa, or BD Canto II analyzer with FACSDiva software. Spherotech AccuCount fluorescent particles were added for cell quantification before analysis on the flow cytometers. Cell doublets were excluded by comparison of the side-scatter width to the forward-scatter area. For analysis of γδ T cells, a 'dump gate' with Ter119, CD19, and F4/80 was used for elimination of nonspecific staining.

PLZF$^+$ and PLZF$^-$ γδ T cells were sorted directly from freshly digested adipose tissue from PLZF^{GFP} mice. Fibroblast subsets were sorted according to the gating scheme outlined in Fig. 6d. Cell sorting was performed on a BD FACSAria Fusion sorter with a 70-µm nozzle. The cell purity was routinely >98%. For RNA analyses, sorted cells were lysed in either TRIzol (Qiagen) or RLT lysis buffer (Qiagen) with 1% β-mercaptoethanol (2-ME, Sigma).

Immunofluorescence. For detection of GFP, epididymal adipose tissue was harvested into 0.02% sodium azide and 5% normal mouse serum in PBS (Jackson ImmunoResearch Laboratories). Adipose tissue mounted on glass slides with Aqua Poly/Mount (Polysciences), and coverslips was imaged with a confocal microscope (Leica TCS SP5).

In vitro stimulations. Adipose tissue was digested as described above, and bulk SVF was stimulated with phorbol 12-myristate 13-acetate (PMA, 50 ng/mL) and ionomycin (1 µg/mL) for 6 h in complete RPMI medium (RPMI supplemented with 10% FBS (Gemini), HEPES (Invitrogen), L-glutamine, penicillin/streptomycin, and 2-ME). Brefeldin A (1:1,000, eBioscience) was added for the last 5 h. Cells were washed twice in 2% FBS in DMEM, surface stained, and fixed and permeabilized with eBioscience Transcription Factor Fix/Perm Buffer to assay cytokine production by γδ T cells.

Primary stromal cells from mouse and human adipose tissue were generated by digesting adipose tissue and expanding bulk cells in six-well plates in DMEM supplemented with 10% FBS (Gemini), 2 mM L-glutamine, 50 µM 2-ME, and antibiotics (penicillin and streptomycin). After 3–5 d, nonadherent cells were washed off, and stromal cells were trypsinized. Stromal cells were plated on day 1 at a density of 5×10^4 cells per well in 24-well plates in 10% FBS-containing medium. Human cells were serum starved on day 2 by being switched to 1% FBS-containing medium. Cells were left unstimulated or were stimulated with the indicated concentrations of TNF (Peprotech), IL-17A (Peprotech), or a combination of the two, for 18 h. Cells were then washed in PBS, and cell lysates were harvested for protein analysis.

Immunoblotting. Whole adipose tissues were homogenized in lysis buffer (50 mM Tris-HCl, 150 mM NaCl, 5 mM EDTA, 1% Triton X-100, protease-inhibitor cocktail (Roche), 500 U/mL benzonase nuclease (Novagen), 1 mM PMSF, 1 mM Na_3VO_4, and 10 mM NaF). Samples were clarified by centrifugation for 15 min at 16,100 *g*. The protein concentration was measured with a BCA protein assay kit (Pierce). 20–50 µg of protein was loaded on 4–20% Mini Protean TGX gradient gels (Bio-Rad). Protein was transferred to 0.2 µm PVDF membranes (Bio-Rad). Membranes were blocked in Tris-buffered saline plus 0.1% Tween 20 (TBS-T) containing 5% BSA or 5% milk for 1 h at 25 °C, then incubated overnight with primary antibodies at 4 °C. Primary antibodies were diluted 1:1,000 in 5% BSA or 5% milk in TBS-T. The primary antibodies used were against UCP1 (Abcam, 10983) and HSP90 (Cell Signaling, 4877, C45G5). Membranes were washed with TBS-T and incubated with HRP-conjugated secondary antibodies (Jackson Immunoresearch; anti-rabbit 111-035-144 and anti-mouse 115-035-003) for 1 h at 25 °C. HRP was activated with Bio-Rad Clarity Western ECL Substrate (Bio-Rad) and visualized with a chemiluminscence detection system (Bio-Rad Chemidoc). The densitometry of blots was analyzed in ImageJ.

ELISA. Processed adipose SVF lysates or stromal cell cultures were diluted 1:2 in reagent diluent (1% BSA in PBS), and IL-33 protein concentrations were quantified with a Mouse/Rat IL-33 Quantikine ELISA kit (M3300, R&D Systems). Adipose SVF lysates were similarly analyzed for IL-2 with a Ready-SET-Go! ELISA kit (eBioscience).

RT–PCR analyses. Tissues were snap frozen in liquid nitrogen and stored at −80 °C until use. Inguinal, epididymal, and brown adipose tissue depots were homogenized in TRIzol reagent (Life Technologies, 15596026) and mixed with chloroform at a ratio of 5:1. After samples were spun, the upper aqueous phase was mixed with the same volume of 70% EtOH, and RNA was isolated with RNeasy Mini Kits (Qiagen, 74104). cDNA was prepared through Quantitect RT–PCR (Qiagen, 205311), and PCR was performed with Brilliant III SYBRGreen (Agilent, 600882) on a Stratagene Mx3000 instrument. The primers used were as follows: *Tbp* (forward, 5′-CTACCGTGAATCTTGGCTGTAAAC-3′; reverse, 5′-AATCAACGCAGTTGTCCGTGGC-3′), *Il10* (forward, 5′-AATAAGCTCCAAGACCAAGG-3′; reverse, 5′-CAGACTCAATACACACTG-3′), *Il33* (forward, 5′-ATGGGAAGAAGCTGATGGTG-3′; reverse, 5′-CCGAGGACTTTTTGTGAAGG-3′), *Ucp1* (forward, 5′-GGCCTCTACGACTCAGTCCA-3′; reverse, 5′-TAAGCCGGCTGAGATCTTGT-3′), *Ppargc1a* (forward, 5′-AGCCGTGACCACTGACAACGAG-3′; reverse, 5′-GCTGCATGGTTCTGAGTGCTAAG-3′), *Dio2* (forward, 5′-TGCCACCTTCTTGACTTTGC-3′; reverse, 5′-GGTTCCGGTGCTTCTTAACC-3′), *Cox7a1* (forward, 5′-AAA CCGTGTGGCAGAGAAGCAG-3′; reverse, 5′-CCCAAGCAGTATAAGCAGTAGGC-3′), *Adrb3* (forward, 5′-AACTGAAACAGCAGACAGGGAC-3′; reverse,

5′-CCCCCATGTACACCCTAGTT-3′), *Th* (forward, 5′-CCAAGGTTCATTGGACGGC-3′; reverse, 5′-CTCTCCTCGAATACCACAGC-3′), *Lipe* (forward, 5′-GCTCATCTCCTATGACCTACGG-3′; reverse, 5′-TCCGTGGATGTGAACAACCAGG-3′), and *Pnpla2* (forward, 5′-GGAACCAAAGGACCTGATGACC-3′; reverse, 5′-ACATCAGGCAGCCACTCCAACA-3′).

Histology. For whole-fat-tissue staining, 5 mm^2 of BAT was fixed in 4% paraformaldehyde in PBS overnight, washed in PBS, and stored in 70% ethanol. Samples were processed and embedded in paraffin and stained with H&E by the Dana Farber Rodent Histopathology Core. For lipid-droplet quantification, histological sections of BAT were placed under a microscope, and images were acquired under 100× magnification. These images in TIFF format were analyzed in the automated Fiji-based Open Source software package Adiposoft. Under 0.485 µm per pixel, a minimum diameter of 20 µm and a maximum diameter of 100 µm were set for the calculation of adipocyte area.

RNA sequencing. RNA was isolated from 800–1,000 cells from sorted γδ T cell populations from *Zbtb16*^{GFP} mice as described. 5 µl of total RNA was placed in wells of a 96-well plate, and RNA sequencing libraries were prepared at Broad Technology Labs at the Broad Institute of Harvard and MIT via the Illumina SmartSeq2 platform. Samples were sequenced on a NextSeq500 instrument with 75-bp paired-end reads to an average depth of 9 million pairs of reads per sample by the Broad Genomics Platform. Reads were mapped to the mouse genome (mm10) with HISAT[43] (0.1.6-beta release). Bam files were sorted and indexed in SAMtools[44] (1.2 release). Assembly, quantification, and normalization were performed in CuffLinks[45] (1.2 release) according to the Tuxedo pipeline[46]. A merged transcriptome constructed from all samples was used as a reference annotation for quantification (by CuffQuant) and normalization (by CuffNorm) stages. Differentially expressed genes between PLZF$^+$ and PLZF$^-$ γδ T cell subsets were identified in CuffDiff[47] (false-discovery rate and adjusted P value <0.1). Genes with calculated FPKM values (according to CuffDiff's pooled dispersion measure) lower than 2^6 in both subsets were removed from the analysis to avoid low noisy measurements. For heat maps, values lower than 1 were replaced by 1, and then the data were $\log_2$ transformed.

Human tissue. Omental adipose tissue was obtained from patients undergoing weight-loss surgery, with the approval of the Brigham and Women's Hospital Institutional Review Board. The tissue was processed similarly to mouse adipose tissue. Matched peripheral blood was also collected for analysis. Informed consent was obtained from all patients, and samples were collected in accordance with BWH ethical regulations. Cultured stromal cell fibroblast lines were generated from visceral preadipocytes (Lonza, PT-5005) and subcutaneous preadipocytes (ATCC, PLS-210-010), and grown in T-75 cm^2 flasks in DMEM supplemented with 10% FBS (Gemini), 2 mM L-glutamine, 50 µM 2-ME, and antibiotics (penicillin and streptomycin).

Statistics. Independent experiments were repeated at least two to three times, and the data are presented as mean ± s.e.m. Statistical significance was determined with two-tailed Student's t test, one-way ANOVA, or two-way ANOVA as indicated. A P value <0.05 was considered statistically significant, and significance is presented as $^*P<0.05$, $^{**}P<0.01$, $^{***}P<0.001$, or $^{****}P<0.0001$. No exclusion of data points or mice was used. Pilot studies were used for estimation of the sample size required to ensure adequate power. GraphPad Prism 6 was used for all statistical analyses.

Reporting Summary. Further information on experimental design is available in the Nature Research Reporting Summary.

Data availability. RNA-seq expression data have been deposited in the Gene Expression Omnibus database under accession number GSE103742. The data that support the findings of this study are additionally available from the corresponding author upon reasonable request.

References

40. Kovalovsky, D. et al. The BTB-zinc finger transcriptional regulator PLZF controls the development of invariant natural killer T cell effector functions. *Nat. Immunol.* **9**, 1055–1064 (2008).
41. Wagers, A. J., Sherwood, R. I., Christensen, J. L. & Weissman, I. L. Little evidence for developmental plasticity of adult hematopoietic stem cells. *Science* **297**, 2256–2259 (2002).
42. Okada, K. et al. Thioesterase superfamily member 1 suppresses cold thermogenesis by limiting the oxidation of lipid droplet-derived fatty acids in brown adipose tissue. *Mol. Metab.* **5**, 340–351 (2016).
43. Kim, D., Langmead, B. & Salzberg, S. L. HISAT: a fast spliced aligner with low memory requirements. *Nat. Methods* **12**, 357–360 (2015).
44. Li, H. et al. The Sequence Alignment/Map format and SAMtools. *Bioinformatics* **25**, 2078–2079 (2009).
45. Trapnell, C. et al. Transcript assembly and quantification by RNA-Seq reveals unannotated transcripts and isoform switching during cell differentiation. *Nat. Biotechnol.* **28**, 511–515 (2010).
46. Trapnell, C. et al. Differential gene and transcript expression analysis of RNA-seq experiments with TopHat and Cufflinks. *Nat. Protoc.* **7**, 562–578 (2012).
47. Trapnell, C. et al. Differential analysis of gene regulation at transcript resolution with RNA-seq. *Nat. Biotechnol.* **31**, 46–53 (2013).

nature research

Corresponding author(s): Michael B. Brenner & Lydia Lynch

☐ Initial submission ☐ Revised version ☒ Final submission

Life Sciences Reporting Summary

Nature Research wishes to improve the reproducibility of the work that we publish. This form is intended for publication with all accepted life science papers and provides structure for consistency and transparency in reporting. Every life science submission will use this form; some list items might not apply to an individual manuscript, but all fields must be completed for clarity.

For further information on the points included in this form, see Reporting Life Sciences Research. For further information on Nature Research policies, including our data availability policy, see Authors & Referees and the Editorial Policy Checklist.

Experimental design

1. Sample size

Describe how sample size was determined.

Pilot studies were used for estimation of the sample size required to ensure adequate power. In some instances, three replicates had to be performed due to the larger signal-to-noise ratio, while conclusions could be made from other experiments where variability was not as great.

2. Data exclusions

Describe any data exclusions.

No data were excluded from the analysis.

3. Replication

Describe whether the experimental findings were reliably reproduced.

All experimental findings were reliably reproduced. In many instances, the experiments have been pooled (as indicated).

4. Randomization

Describe how samples/organisms/participants were allocated into experimental groups.

Littermate mice were ear tagged and genotyped in order to determine genetic genotype and generate experimental groups. Each cohort of littermate mice were housed in the same cage to ensure no contribution of microbiome differences owing to strain.

5. Blinding

Describe whether the investigators were blinded to group allocation during data collection and/or analysis.

Investigators were not blinded during data collection and analysis.

Note: all studies involving animals and/or human research participants must disclose whether blinding and randomization were used.

6. Statistical parameters

For all figures and tables that use statistical methods, confirm that the following items are present in relevant figure legends (or in the Methods section if additional space is needed).

n/a	Confirmed
☐	☒ The exact sample size (*n*) for each experimental group/condition, given as a discrete number and unit of measurement (animals, litters, cultures, etc.)
☐	☒ A description of how samples were collected, noting whether measurements were taken from distinct samples or whether the same sample was measured repeatedly
☐	☒ A statement indicating how many times each experiment was replicated
☐	☒ The statistical test(s) used and whether they are one- or two-sided (note: only common tests should be described solely by name; more complex techniques should be described in the Methods section)
☐	☒ A description of any assumptions or corrections, such as an adjustment for multiple comparisons
☐	☒ The test results (e.g. *P* values) given as exact values whenever possible and with confidence intervals noted
☐	☒ A clear description of statistics including central tendency (e.g. median, mean) and variation (e.g. standard deviation, interquartile range)
☐	☒ Clearly defined error bars

See the web collection on statistics for biologists for further resources and guidance.

Software

Policy information about availability of computer code

7. Software

Describe the software used to analyze the data in this study.	FIJI-based Open Source software package Adiposoft was used to analyze histological sections. ImageJ was used for immunoblot densitometry analysis. Cufflinks and Cuffdiff was used for RNA sequencing analysis. CLAMS data was analyzed using a custom R package for indirect calorimetry experiments. GraphPad Prism 6 was used for all other analysis.

For manuscripts utilizing custom algorithms or software that are central to the paper but not yet described in the published literature, software must be made available to editors and reviewers upon request. We strongly encourage code deposition in a community repository (e.g. GitHub). *Nature Methods* guidance for providing algorithms and software for publication provides further information on this topic.

Materials and reagents

Policy information about availability of materials

8. Materials availability

Indicate whether there are restrictions on availability of unique materials or if these materials are only available for distribution by a for-profit company.	anti-TCR Vδ3 was custom made in Labpan (Europe).

9. Antibodies

Describe the antibodies used and how they were validated for use in the system under study (i.e. assay and species).	Single-cell suspensions were incubated with Fc receptor–blocking antibody (14-0161-82; eBioscience) before being stained on ice. Dead cells were excluded with a live/dead Zombie Aqua stain (BioLegend). For intracellular transcription factor staining, cells were fixed and permeabilized using the eBioscience Transcription Factor Fix/Perm Buffer. Mouse antibodies were as follows: anti-CD45 (30-F11), anti-CD45.1 (A20), anti-CD45.2 (104), anti-CD27 (LG.3A10), anti-CD69 (FN50), anti-CD44 (BJ18), anti-CD127 (A019D5), anti-CD4 (RM4-5), anti-CD8a (53-6.7), anti-TCRb (H57-597), anti-KLRG1 (2F1/KLRG1), anti-pdpn (8.1.1), anti-CD26 (H194-112FC), and anti-CD31 (390) were all purchased from BioLegend. Anti-Ter119 (TER-119), anti-F4/80 (BM8), anti-CD19 (ID3), anti-γδ TCR (GL3), anti-CD3e (500A2), anti-PLZF (Mags.21F7), anti-Foxp3 (FJK-16s), anti-ST2 (RMST2-2), anti-Tbet (4B10), anti-Rorγt (B2D), anti-TNF (MP6-XT22), anti-IL17A (17B7), anti-IFNγ (XMB1.2), anti-PDGFRα (APA5), anti-IL17RA (PAJ-17R), and streptavidin-APC were all purchased from eBioscience. To stain for Vγ6+ cells, GL3 (anti-TCRγδ) and 17D1 (anti-Vγ5Vδ1) antibodies were used as previously described30. Anti-Vγ4 (UC3-10A6) was purchased from BD Pharmingen. Biotinylated anti-cad11 was generated in house. Mouse PBS-57-loaded CD1d tetramers were from the NIH tetramer facility. Human antibodies were as follows: anti-TCR Vδ1 (REA173) and anti-TCR Vδ2 (123R3) were purchased from Miltenyi Biotec. Anti-CD3 (UCHT1) was purchased from Biolegend. anti-TCR Vδ3 was custom made in Labpan (Europe). Antibodies were used at a concentration of 1:100 - 1:200 per recommendation by the respective manufacturer's website.

10. Eukaryotic cell lines

a. State the source of each eukaryotic cell line used.	3T3L1 fibroblasts were acquired from ATCC. Primary subcutaneous pre-adipocytes - Normal-Human ATCC PLS-210-010. Primary visceral pre-adipocytes from Lonza - Normal-Human Cat# PT-5005 // #000000029918 / Lot# 313366.
b. Describe the method of cell line authentication used.	None of the cell lines have been authenticated.
c. Report whether the cell lines were tested for mycoplasma contamination.	Cell lines were not tested for mycoplasma infection.
d. If any of the cell lines used are listed in the database of commonly misidentified cell lines maintained by ICLAC, provide a scientific rationale for their use.	No commonly misidentified cell lines were used.

Animals and human research participants

Policy information about studies involving animals; when reporting animal research, follow the ARRIVE guidelines

11. Description of research animals

Provide details on animals and/or animal-derived materials used in the study.

C57BL/6J (WT), Il17a–/–, Tcrd–/–, and Il17aGFP mice were purchased from Jackson Laboratory. Littermates were bred and maintained in specific-pathogen-free animal facilities at Brigham and Women's Center for Comparative Medicine. In almost all experiments, male mice aged anywhere from 5-25 weeks were used. The exact age of the mice is specified in each appropriate section in the figure legends of the manuscript. PLZF reporter mice (Zbtb16GFP mice) and Zbtb16–/– were generated in the Sant'Angelo laboratory as previously described3,40. Vgamma4/6–/– (Vg4/6–/–) mice were a kind gift from R. O'Brien30. All animal work was approved by and was in compliance with the Institutional Animal Care and Use Committee guidelines of Brigham and Women's Hospital and Harvard Medical School.

Policy information about studies involving human research participants

12. Description of human research participants

Describe the covariate-relevant population characteristics of the human research participants.

Omental adipose tissue was obtained from patients undergoing weight-loss surgery with approval of the Brigham and Women's Hospital Institutional Review Board. Tissue was processed similar to mouse adipose tissue. Matched peripheral blood was also collected for analysis. Informed consent was obtained from all patients and samples collected following BWH ethical regulations.

nature research

Corresponding author(s): Michael B Brenner & Lydia Lynch

☐ Initial submission ☐ Revised version ☒ Final submission

Flow Cytometry Reporting Summary

Form fields will expand as needed. Please do not leave fields blank.

Data presentation

For all flow cytometry data, confirm that:

☒ 1. The axis labels state the marker and fluorochrome used (e.g. CD4-FITC).

☒ 2. The axis scales are clearly visible. Include numbers along axes only for bottom left plot of group (a 'group' is an analysis of identical markers).

☒ 3. All plots are contour plots with outliers or pseudocolor plots.

☒ 4. A numerical value for number of cells or percentage (with statistics) is provided.

Methodological details

5. Describe the sample preparation.	Adipose tissue was carefully excised, minced, and digested with 1mg/ml collagenase type 2 (Worthington #LS004188) in RPMI (Life Technologies) for 25min at 37°C, with shaking. Cells were passed through a 70µm cell strainer, washed, and centrifuged for 5min at 300xg to pellet the stromal-vascular fraction from floating mature adipocytes. For the preparation of single-cell suspensions of liver, the organ was perfused via the portal vein with 10ml PBS and mashed through a 70µm cell strainer. Liver samples underwent enrichment for lymphocytes by centrifugation using a Percoll gradient. Spleens were strained through a 70µm cell strainer and spun. Pellets from all tissues were subjected to red blood cell lysis and subsequently resuspended in flow cytometry buffer (2% FBS and 0.02% NaN3 in phenol-free DMEM) for further staining.
6. Identify the instrument used for data collection.	BD FACSAria Fusion, BD Fortessa, or BD Canto II analyzer
7. Describe the software used to collect and analyze the flow cytometry data.	FACSDiva software and FlowJo
8. Describe the abundance of the relevant cell populations within post-sort fractions.	Gamma delta T cells in adipose tissue comprise 9-15% of the CD3e+ T cells. Sorted endothelial cells (CD31+) are 20-40% of the CD45- population in adipose tissue. Pdpn+PDGFRa- cells are 4-8% of the CD45- population. and PDGFRa+cells are 50-65% of the CD45- cells in adipose tissue.
9. Describe the gating strategy used.	Gamma delta T cells were identified using a lymphocyte gate in the FSC/SSC, CD45+ selection, and CD19-Ter119-F4/80- dump channel. From there CD3e and TCRd were used to identify the gamma delta T cell populations. PLZF reporter mice were used to sort PLZF+ CD3bright and PLZF- CD3dim populations for RNAseq. Stromal cells were gated based on FSC (>40K) and SSC. CD45- cells were further isolated and CD31 and gp38 (pdpn) were used to distinguish endothelial cells. Of the pdpn+ fibroblasts, PDGFRa was used to distinguish preadipocytes (PDGFRa+) and Pdpn-hiPDGFRa- cells.

Tick this box to confirm that a figure exemplifying the gating strategy is provided in the Supplementary Information. ☒